



1 Diatom–environment relationships and limnological variability: an 2 updated quantitative tool for palaeoclimatology on sub-Antarctic 3 Macquarie Island

4 Caitlin A. Selfe¹, Karina Meredith², Liza McDonough², Justine Shaw¹, Stephen J. Roberts³, Krystyna M.
5 Saunders^{2,4}

6
7 ¹ Securing Antarctica's Environmental Future, Queensland University of Technology, Brisbane, 4000,
8 Australia

9 ² Securing Antarctica's Environmental Future, Environment Research and Technology Group, Australian
10 Nuclear Science and Technology Organisation, Lucas Heights, 2234, Australia

11 ³ British Antarctic Survey, Cambridge, CB3 0ET, United Kingdom

12 ⁴ Institute for Marine and Antarctic Studies, University of Tasmania, Hobart, 7004, Australia

13
14 Correspondence to: Caitlin A. Selfe (caitlin.selfe@hrd.qut.edu.au)

15 **Keywords:** Diatoms, Electrical conductivity, sub-Antarctic, Macquarie Island, Transfer function, Southern
16 Hemisphere westerly winds, Palaeoclimate, Limnology



17 **Abstract.** Sub-Antarctic Macquarie Island is ideally located for reconstructing past variations in Southern
18 Hemisphere westerly wind strength. Diatoms are a valuable palaeolimnological tool on sub-Antarctic
19 islands, providing a means to reconstruct past climate and environmental changes. Diatom communities
20 are sensitive to changes in lake electrical conductivity (EC) linked to westerly wind–driven sea-spray
21 inputs on Macquarie Island, and diatom–conductivity models have previously been used to infer past
22 westerly wind variability. Here we present new diatom data from 52 lakes to assess diatom–environment
23 relationships and develop an updated diatom–conductivity model for Macquarie Island. Seasonal and
24 multi-year water chemistry and isotope data were analysed to assess temporal variability in
25 hydrochemical processes and the influence of evaporation, ensuring the resulting diatom-conductivity
26 model reflects external climatic drivers rather than local dynamics. Statistically robust transfer functions
27 were developed for EC (bootstrapped $r^2 = 0.80$, RMSEP = 0.40), while pH and temperature had weaker
28 predictive performance. For EC, weighted averaging and maximum-likelihood approaches performed
29 comparably, although the former showed reduced predictive power at high EC where low species
30 turnover and nutrient collinearity affected accuracy. This quantitative-diatom model combined with
31 understanding of hydrogeochemical processes provides an improved basis for reconstructing past
32 Southern Hemisphere westerly wind variability, which can be applied in future palaeoclimate studies on
33 Macquarie Island.



34 1 Introduction

35 The Southern Ocean region exerts a strong influence on Southern Hemisphere and global climates
36 (Jones et al., 2016; Fogt & Marshall, 2020). Sub-Antarctic islands are among the few landmasses located
37 in the Southern Ocean, making them important sites for understanding the past and future role of the
38 Southern Ocean on climate variability. The Southern Hemisphere westerly winds (SHW) are a major
39 driver of Southern Hemisphere mid- to high-latitude climates, modulating ocean circulation, mid-latitude
40 temperature and precipitation regimes, and the efficiency of the Southern Ocean carbon sink (Gillett et
41 al., 2006; Le Quéré et al., 2009; Fletcher et al., 2021; Thomas et al., 2025). Instrumental data show that
42 in recent decades the SHW have intensified and shifted poleward in response to warming (Marshall,
43 2003; Fogt & Marshall, 2020). These changes have been linked to an increase in net outgassing of
44 carbon dioxide (CO_2) from deep-storage reservoirs in the Southern Ocean, with significant implications
45 for future atmospheric CO_2 levels and global temperatures (Goyal et al., 2021; Nicholson et al., 2022;
46 Mongwe et al., 2024; Olivier & Haumann, 2025). Understanding long-term SHW variability is key to
47 assessing the impacts of SHW dynamics under future climate warming scenarios.

48

49 Diatoms are highly sensitive to environmental changes and are widely used as proxies in
50 palaeolimnology to infer climate and environmental changes (Roberts et al., 2000; Verleyen et al., 2003;
51 Sterken et al., 2008; Recasens et al., 2015). Previous work on sub-Antarctic Islands has demonstrated
52 that aquatic diatom communities are significantly influenced by changes in salinity (inferred from
53 electrical conductivity (EC)), allowing quantitative diatom-conductivity models to be developed
54 (Gremmen et al., 2007; Saunders et al., 2009; 2015; 2018; Van Nieuwenhuyze, 2020; Menviel et al.,
55 2023). On sub-Antarctic islands, lake water salinity changes are largely controlled by wind-driven sea
56 spray aerosol (SSA) inputs with increased inputs occurring when winds are stronger and vice versa
57 (Evans, 1970; Buckney & Tyler, 1974; Saunders et al., 2009, 2015). Based on this, diatom-conductivity
58 transfer functions have been used to infer past SHW intensity on Macquarie (Saunders et al., 2018) and
59 Marion Island (Perren et al., 2020).

60

61 Earlier studies on Macquarie Island have analysed diatom-environment relationships (McBride, 2009;
62 Saunders et al., 2009) and their application as palaeoenvironmental and climate proxies (Keenan, 1995;
63 Saunders et al., 2013; 2018). However, from the late 1900s to early 2000's overgrazing from increasing



64 invasive rabbit populations resulted in widespread ecosystem degradation, including erosion, vegetation
65 loss, and altered organic inputs into lakes. This affected aquatic ecosystems and diatom diversity
66 (Marchant et al., 2011; Saunders et al., 2013). The Macquarie Island Pest Eradication Programme
67 successfully eradicated all invasive vertebrates (principally rabbits) from the island, triggering substantial
68 ecosystem recovery (Springer, 2018; Fitzgerald et al., 2021). Reassessing diatom–environment
69 relationships under current post-eradication (recovery) conditions is necessary, because earlier studies
70 were conducted during a period of disturbance related to introduced invasive vertebrates rather than
71 when the island was in a natural state (Saunders et al., 2013). Developing new diatom models based on
72 recovered conditions may better represent pre-invasion baseline communities, improving the accuracy
73 and ecological relevance of palaeolimnological reconstructions. Furthermore, incorporating revised
74 taxonomy and newly identified species will enhance the model's ecological resolution and predictive
75 performance.

76

77 Understanding the processes that drive lake water chemistry, such as precipitation, evaporation,
78 groundwater inputs, and nutrient cycling, and how they vary across temporal and spatial scales is
79 essential when interpreting diatom–environmental relationships. Hydrochemical analyses of lakes
80 across Macquarie Island show that dominant processes vary locally, and lakes can be classified as
81 predominantly influenced by SSAs, catchment processes (i.e., with greater water-rock interaction), or
82 precipitation (i.e., more dilute lake waters) (Meredith et al., 2022). Sea-spray-influenced lakes occur near
83 the west coast and on the western edge on the Macquarie Island plateau, where exposure to the SHW
84 is greatest. In contrast, catchment-influenced lakes with higher terrestrial ion concentrations are found
85 at lower elevations, and rainfall-influenced lakes with low ion concentrations occur at higher elevations.
86 This hydrogeochemical understanding supports the hypothesis that for lakes near the west coast,
87 including those on the western edge of the plateau, EC-related diatom variation on Macquarie Island
88 primarily reflects SHW-driven sea-spray inputs rather than local hydrological or geochemical controls.

89

90 While these data provide valuable insight into spatial variability, it is necessary to quantify temporal
91 variability in hydrogeochemical processes, particularly evaporation, to assess how seasonal, interannual,
92 and longer-term changes modify ion concentrations in lakes, including those derived from SSA.
93 Establishing seasonal and multi-year lake water hydrogeochemical datasets will enhance confidence in
94 proxy interpretations and form a foundation for long-term monitoring of Macquarie Island lakes. Such



95 research is rare worldwide, and has not yet been undertaken on other sub-Antarctic Islands, making this
96 study important for understanding how sub-Antarctic Island ecosystems will respond to future climate
97 and environmental changes, which are experiencing rapid climatic and ecological shifts (le Roux &
98 McGeoch, 2008; Lee & Chown, 2016; Nel et al., 2023).

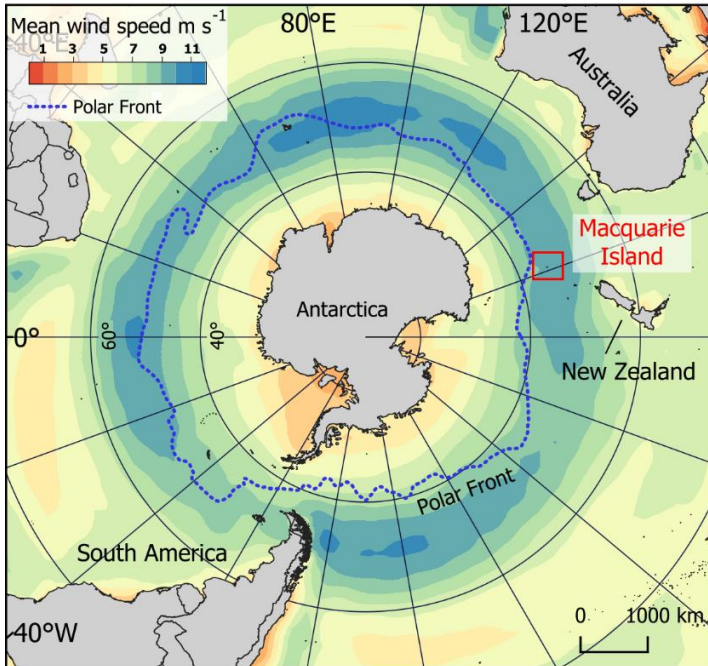
99

100 Here, we present new data from lakes on Macquarie Island quantifying post-pest eradication
101 relationships between surface-sediment diatom communities and environmental conditions. Using
102 comprehensive water chemistry datasets from 2018 and 2022–23, we examine seasonal and interannual
103 variability to develop updated diatom–environment transfer functions. This integrated approach
104 strengthens the application of diatom-based proxies and provides a first step towards long-term
105 monitoring of sub-Antarctic lake systems.

106 **2 Methods and Materials**

107 **2.1 Study area: Macquarie Island**

108 Macquarie Island (54°50'S, 158°85'E) is a small sub-Antarctic island (128 km²) located in the Southern
109 Ocean just north of the polar front, 1200 km south-west of New Zealand and 1300 km from the Antarctic
110 continent (Fig. 1a). It is one of the few landmasses within the Polar Frontal Zone and modern core SHW
111 belt (50–55°S; Fig.1), making it ideally suited to study past and current changes in temperature, the
112 SHW, and precipitation. It has a harsh, cool, wet, oceanic climate representative of the core SHW belt,
113 with low seasonality and high wind velocities (Selkirk et al., 1990). The SHW prevail almost exclusively
114 from the west and north-west with a mean annual wind speed of 35km/h and gusts reaching 185km/h
115 (between 1948-2025; BOM, 2025). The continual dominance of the SHW drive environmental and
116 ecosystems responses on a west-to-east gradient across the island (Chau et al., 2019; Meredith et al.,
117 2022), including the deposition and accumulation of wind-blown inputs such as sea spray and
118 minerogenic aerosols (Buckney & Tyler, 1974; Saunders et al., 2009). Mean annual temperature ranges
119 from 3.1–6.6°C, and the island experiences high annual rainfall of > 1000 mm with > 317 rainy days yr⁻¹
120 (between 1948–2025; BOM 2025). Rainfall has increased in recent decades with a higher frequency of
121 intense rainfall events, mostly occurring during winter, which are then accompanied by drier windier
122 summers (Andersen et al., 2009; Kong et al., 2025). Persistent cloud cover over the island results in low
123 light levels and sunshine hours per day (average 2.4 h from 1948–2022; BOM, 2025).



124
125 **Figure 1: Location of Macquarie Island in the Southern Ocean and modern core SHW belt (50–55S°) with mean wind**
126 **speed shown.**

127 Macquarie Island is geologically unique, being the only location worldwide where an intact marine
128 ophiolite sequence of oceanic crust and upper mantle is exposed above sea level (Davis, 1987). The
129 island is composed mostly of pillow basalts with interspersed flows of massive basalt (Selkirk et al.,
130 1990). Dolerite, ultrabasics and intrusives are also present but are confined to the northern third of the
131 island (Mawson 1943). As widespread glaciation did not occur during the global Last Glacial Maximum
132 (26–20 ka), marine, periglacial and subaerial erosional, rather than glacial processes, shaped the island
133 as well as lake formation and ontogeny. The island is fringed by a low coastal terrace leading to steep-
134 sided slopes (20–40°) that rise to form the island plateau sitting at ~200–400 m asl (Selkirk et al., 1990;
135 McBride & Selkirk, 1998).

136

137 The island has numerous shallow and deep lakes and ponds across the plateau and coastal terrace (Fig.
138 2). High accumulation of surface water and a high water-table at or very near the surface lead to the
139 formation of extensive mires across the island (Löffler, 1984). While lake edges can form thick ice cover
140 during winter, complete freezing of the lakes is not typically observed (Evans, 1970; Selkirk-Bell &



141 Selkirk, 2013). The island is vegetated by bryophytes, tussock grass, herbs and sedges, with no shrub
142 or tree species present (Selkirk et al., 1990).

143 **2.2 Data collection**

144 Surface sediments and water samples were collected from lakes on Macquarie Island during the 2022–
145 23 austral summer (referred to as 2022). Sites were selected to replicate those sampled in 2018 that
146 were published by Meredith et al. (2022). Lake surface sediments were collected from 30 plateau (inland)
147 sites for diatom analyses (lake ID = LK). Surface sediments (top 2 cm) were collected from each site
148 using a long-handled scoop from < 1 m water depth. An additional 17 coastal and five plateau sites
149 sampled in 2006 (lake ID = S; Saunders et al. 2009) were included in the diatom dataset to extend the
150 EC and nutrient gradients of the updated dataset, totalling 52 samples (Fig. 2a). Two lakes were
151 replicated in the 2006 and 2022 seasons (S9 = LK40, S18 = LK2; Fig. 2a).

152

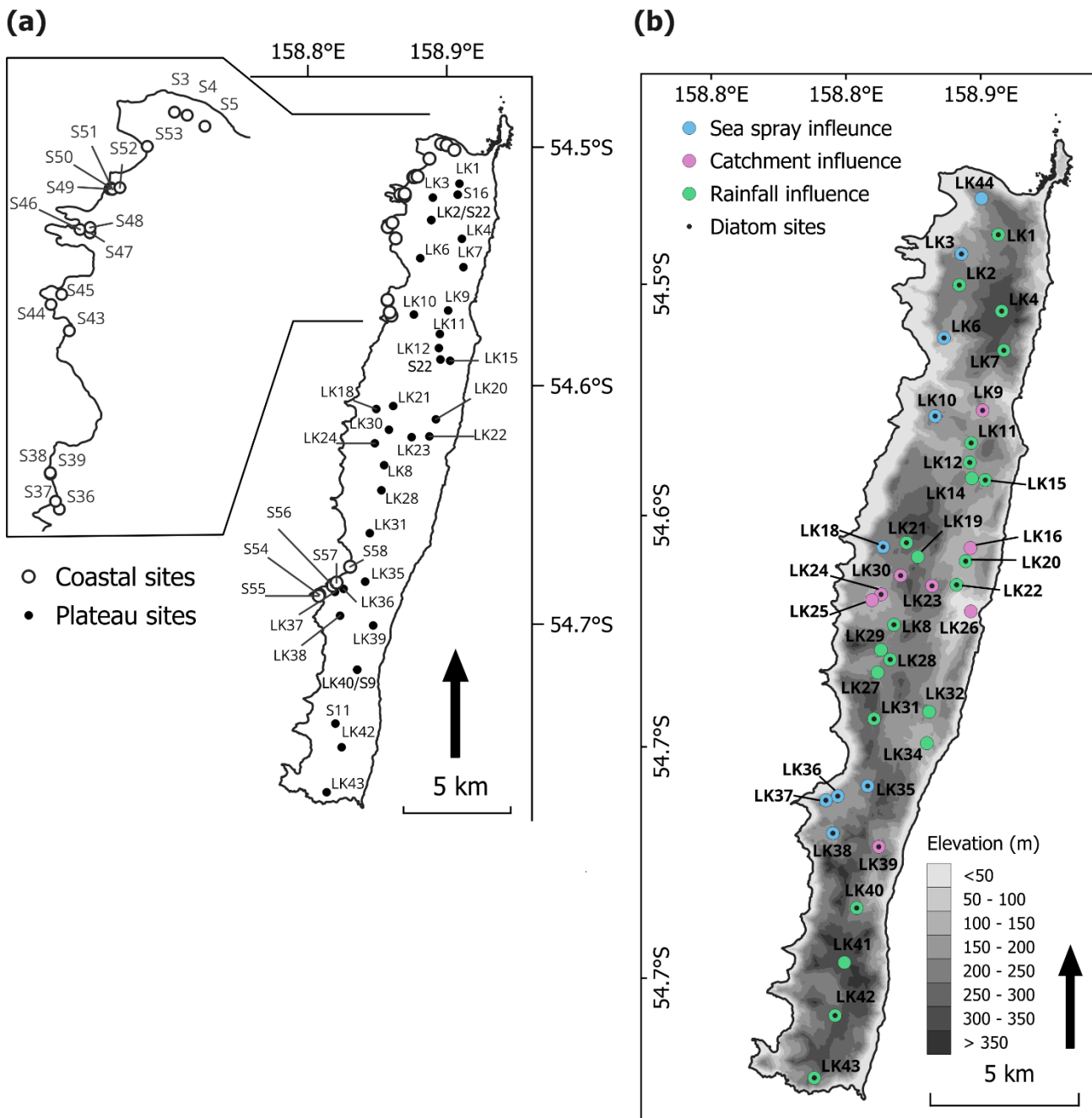
153 Lake water general parameters were measured in-situ at each site, including temperature, EC, dissolved
154 oxygen (DO) and pH using a YSI ProQuatro Multiparameter Meter, with calibration performed prior to
155 every sampling trip. DO was calibrated in water-saturated air following YSI manufacturer protocols.
156 Conductivity was calibrated using a $1413 \mu\text{S cm}^{-1}$ standard solution, and pH was calibrated using a
157 three-point procedure with pH 4.0, 7.0, and 10.0 buffer solutions. Water samples were collected at all
158 diatom sampling sites to measure total oxidised nitrogen (TON), phosphate (PO_4^{3-}), and silica (Si).
159 Additional water samples were collected from 40 plateau sites for water chemistry analysis (Fig. 2b),
160 including major ions and stable water isotopes (oxygen ($\delta^{18}\text{O}$) and hydrogen ($\delta^2\text{H}$)). Each site was
161 sampled three times across the 2022–23 season (November, December to January, and February). All
162 water samples were collected from ~20 cm below the water surface and were filtered in-situ with 0.45
163 μm polyethersulfone filters into High Density Poly-Ethylene (HDPE) bottles following the method
164 described by Meredith et al. (2009). Water samples were refrigerated (4°C) until analysis.

165

166 Major ions, and oxygen ($\delta^{18}\text{O}$) and hydrogen ($\delta^2\text{H}$) stable isotopes were analysed at the Australian
167 Nuclear Science and Technology Organisation (ANSTO). Cations and anions were analysed using
168 inductively coupled plasma-atomic emission spectrometry (ICP-AES). $\delta^{18}\text{O}$ and $\delta^2\text{H}$ stable isotopes
169 were analysed with a Picarro L2130-i Cavity Ring-Down Spectrometer. Values were reported as per mill



170 (%) deviations relative to the international standard V-SMOW (Vienna Standard Mean Ocean Water),
171 with a reproducible precision of ± 0.2 and $\pm 1.0\%$, respectively.



172 Figure 2: Maps showing lake sites across Macquarie Island, a) Diatom surface sediment sites (coastal sites were originally sampled
173 by Saunders et al. (2009); b) Lake water chemistry sites. Colours show lake types, based on dominate hydrogeochemical processes,
174 identified by Meredith et al., (2022). Black dots indicate that the site is included in the diatom dataset.



175 Nutrient data from 2006 samples (filtered at 0.45µm) measured soluble reactive phosphate (SRP), TON
176 (nitrate (NO₃) + nitrite (NO₂)), and silicate (Si) using an Alpkem Autoanalyser (Continuous Flow Solution
177 Analyser), representing the operationally defined dissolved inorganic (and therefore readily bioavailable)
178 fractions of total N, P, and Si. In contrast, the 2022 dataset measured TON, PO₄³⁻, and Si ions using
179 ICP-AES at ANSTO on filtered, undigested waters, with results reported as the corresponding inorganic
180 species and concentrations consistently at or near detection limits. Despite methodological differences,
181 the two approaches yield consistently low and broadly comparable concentrations in the two replicate
182 lakes across sampling trips: for S9/LK40, PO₄³⁻ concentrations were 0.002 mg L⁻¹ (autoanalyser) and <
183 0.01 mg L⁻¹ (ICP-AES), and TON concentrations were 0.006 mg L⁻¹ (autoanalyser) and < 0.06 mg L⁻¹
184 (ICP-AES); for S18/LK2, PO₄³⁻ concentrations were 0.004 mg L⁻¹ (autoanalyser) and < 0.01 mg L⁻¹
185 (ICP-AES), and TON concentrations were 0.005 mg L⁻¹ (autoanalyser) and < 0.06 mg L⁻¹ (ICP-AES).
186 Furthermore, if the 2022 analyses targeted the same reactive fractions measured in 2006, the results
187 would still fall below or close to detection limits.

188 **2.3 Diatom preparation and identification**

189 Diatom preparation followed methods described by McBride (2009). Cleaned diatom solutions were
190 mounted onto slides using Norland Optical Adhesive 61. At least 300–400 frustules were counted per
191 sample, using Differential Interference Contrast (DIC) and oil immersion at 1000x magnification on a
192 Zeiss Axioskope microscope, mounted with a TOUPTEK camera (U3CMOS). Species identification was
193 primarily based on sub-Antarctic taxonomy described in Van de Vijer et al. (2002); Sterken et al. (2015);
194 Sabbe et al. (2019); and Van de Vijver (2019). Species were photographed and documented (see
195 Supplementary Material for an illustrated species catalogue).

196 **2.4 Statistical analyses**

197 **2.4.1 Water chemistry**

198 The lake water chemistry dataset was comprised of *in-situ* general parameters, major ion concentrations
199 and δ¹⁸O and δ²H values from 2018 (Meredith et al. 2022) and 2022 (this study) to understand temporal
200 variation across the island. Data from 2018 (January to February) are referred to as sampling event 1
201 (E1) and sampling from the 2022 season as E2 (November), E3 (December to January), and E4
202 (February). Shapiro–Wilk tests showed that isotope data were normally distributed ($p > 0.05$), whereas



203 general parameters and ion concentrations deviated significantly from normality ($p < 0.05$).
204 Consequently, parametric tests (ANOVA, t-test, Tukey's HSD) were applied to isotope data, and non-
205 parametric tests (Kruskal-Wallis, pairwise Wilcoxon) to general parameters ion data. A Principal
206 Component Analysis (PCA) with z-score standardised data was performed to explore relationships
207 between variables and assess the consistency of lake types identified by Meredith et al., (2022; Fig. 2b).

208 **2.4.2 Diatom model**

209 Ordination methods were used to describe variation in the diatom dataset, explore diatom-environment
210 relationships, and identify unique variance explained by environmental variables. Environmental
211 variables included were EC, temperature, DO, pH, TON, PO_4^{3-} , and Si, additional major ions were not
212 included as these data were not available for 2006 sites. Weighted Averaging (WA) was applied to
213 dominant species to determine ecological optima and tolerance. Together WA, Weighted Averaging
214 Partial Least Squares (WAPLS), and Maximum Likelihood (ML) models were used to develop diatom
215 transfer functions, with cross-validation used to assess model robustness.

216

217 The relative abundance of each diatom species in each sample was calculated as the percentage of the
218 total number of frustules counted per sample. Species occurring at $\leq 1\%$ relative abundance were
219 excluded from the dataset. A full species list can be found in Supplementary Material. Nutrient values
220 that were below the limit of detection were substituted with the respective detection limit value (PO_4^{3-} =
221 0.01 mg L^{-1} , Si = 0.1 mg L^{-1} , TON = 0.06 mg L^{-1}). Environmental variables were screened for skewness,
222 with temperature, EC, PO_4^{3-} , Si, and TON $\log(x+1)$ transformed.

223

224 PCA was performed on transformed environmental data to identify the primary gradients of
225 environmental variation across sites. Detrended Correspondence Analysis (DCA) with detrending by
226 segments and downweighting of rare species was performed on untransformed species data to
227 determine whether species distributions were linear or unimodal. As the DCA axis 1 gradient length (8.2
228 deviation units) was > 4 , unimodal ordination methods were deemed appropriate (Ter Braak & Prentice,
229 1988). Species data were $\log(x+1)$ transformed for remaining analysis.

230

231 A series of Canonical Correspondence Analyses (CCA) were then performed with forward selection, and
232 scaling focused on inter-species distances, biplot scaling and downweighting of rare species. Variance



233 Inflation Factors (VIF) of environmental variables were used to assess collinearity. As no variables had
234 a VIF >10, none were excluded. A full CCA, with all environmental variables included, was first performed
235 to quantify the total amount of species–environment variation explained by the full set of variables. A
236 series of independent and partial CCAs with variance partitioning were performed to constrain analyses,
237 assess the relative explanatory power, and assess the unique and shared variance contributions of each
238 variable. Individual CCAs, of each variable alone, estimate the marginal (unconstrained) explanatory
239 power (i.e., how much variation a single variable explains when considered alone, without accounting
240 for correlations with other variables). Partial CCAs assess the unique (conditional) contribution of each
241 environmental variable after statistically controlling for all remaining variables. This analysis isolates the
242 variance uniquely attributable to each predictor and identifies variables whose explanatory power is
243 driven by covariation with others. Finally, variance partitioning was used to decompose the total
244 explained variation into unique and shared fractions, allowing assessment of how much variation was
245 due to individual predictors versus overlapping environmental gradients. Permutation test results ($p >$
246 0.05), CCA coefficients and lambda ratios (λ_1/λ_2) of the first constrained eigenvalue (λ_1) to the second
247 unconstrained eigenvalue (λ_2) were used to identify the environmental variables most appropriate for
248 quantitative inference models. As a guide, high λ_1/λ_2 ratios are necessary for a variable to have enough
249 explanatory power to be included in quantitative inference models (Ter Braak & Prentice, 1988; Juggins,
250 2013). All ordination analyses were performed using the *vegan* package version 2.7-1 (Oksanen et al.,
251 2013) in R (R Core Team, 2024).

252

253 ML and iterations of inverse (_{INV}) and classical (_{CLA}) WA models with and without tolerance downweighting,
254 and WAPLS with up to five components were assessed to provide the best performing transfer functions.
255 These methods were applied because they capture different aspects of species–environment
256 relationships: WA provides a simple unimodal estimator; WAPLS allows more complex responses
257 through latent components; and ML emphasises taxa with narrow ecological tolerances. Using multiple
258 approaches therefore offers complementary strengths and helps identify the most reliable and robust
259 model through cross-validation. All models were performed with bootstrapping and 100 iterations. Model
260 r^2 , bootstrapped r^2 (r_{boot}^2), root mean square error (RMSE) and root mean square error of prediction
261 (RMSEP) values were used to assess performance. RMSEP and r_{boot}^2 performance was favoured over
262 r^2 and RMSE. RMSEP between WAPLS components was also used to assess overfitting. WA and
263 WAPLS-1 results are often similar as WAPLS is built upon the same weighted-averaging framework



264 as WA (ter Braak & Juggins, 1993). When this was the case and WAPLS components did not improve
265 performance, WA was favoured as it is the simplest model. Software program C2 version 1.8 (Juggins,
266 2003) was used to develop all transfer functions.

267 3 Results

268 3.1 Lake water chemistry

269 Analysis of 40 plateau lakes on Macquarie Island showed that lake water general parameters (EC, pH
270 and DO), and nutrients, did not vary significantly across the 2022 sampling events (E2-4; Table 1).
271 Temperature was seen to vary, being significantly lower in E2 compared to E3 and E4. Lakes are slightly
272 acidic (pH 5.7) to slightly alkaline (pH 9.14). Mean EC ranged from 126–261 $\mu\text{S cm}^{-1}$, with a decrease
273 in EC from west to east across the island. Lakes are oxic (DO = 8.64–12.61 mg L⁻¹) and oligotrophic,
274 with PO₄³⁻ and TON concentrations under or close to detection limits (< 0.01–0.02 mg L⁻¹ and < 0.06–
275 0.1 mg L⁻¹, respectively). Similarly, comparison with 2018 plateau lakes showed no significant difference
276 across all lake water general parameters, excluding temperature, indicating generally stable conditions
277 in plateau lakes across years. However, a comparison between plateau lakes measured in 2022 and
278 coastal lakes in 2006 did show significant differences ($p < 0.05$). Coastal sites in 2006 were generally
279 eutrophic with higher nutrient ranges (TON = 0.007–4.636 mg L⁻¹, PO₄³⁻ = 0.1–9.9 mg L⁻¹, and Si 0.07–
280 2.71 mg L⁻¹), and higher EC (406–1482 $\mu\text{S cm}^{-1}$), while temperature, DO and pH were similar (Table 1;
281 see Supplementary Table S1 and S2 for full results).

282

283 Major ion analysis of the 40 plateau lakes showed that, although dilute in concentration, Cl (1.1–3.7
284 mmol L⁻¹) and Na (0.9–2.6 mmol L⁻¹) dominate the ionic composition of all lake waters (Table 2; see
285 Supplementary Table S3 for full cation and anion results). All lakes showed similar ionic ratios to
286 seawater for SO₄, Cl, Mg, and Na, suggesting a marine origin. Seawater ionic ratios diverged for K, Ca
287 and F for some lakes, while SiO₂ was higher in all lakes, suggesting additional sources for these ions.
288 (Fig. 3).



289 Table 1: Summary table of lake water general parameters and nutrient data. Temp. = temperature, DO = dissolved oxygen, EC =
 290 electrical conductivity, Si = silicate, PO_4^{3-} = phosphate, TON = total oxidised nitrogen.

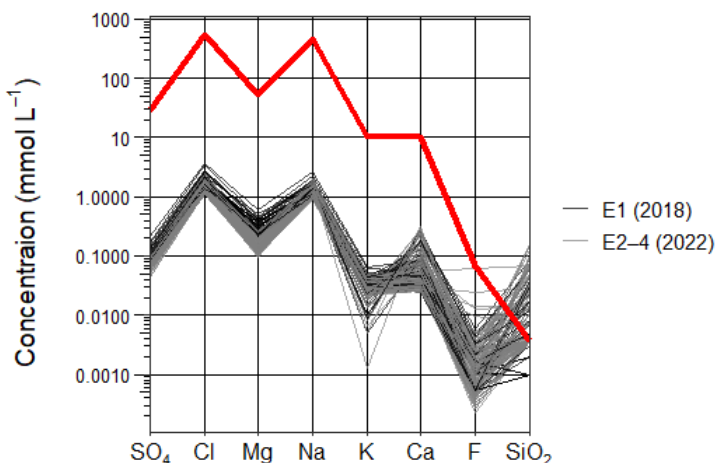
| | Temp. (°C) | DO (mg L ⁻¹) | EC ($\mu\text{s cm}^{-1}$) | pH | Si (mg L ⁻¹) | TON (mg L ⁻¹) | PO_4^{3-} (mg L ⁻¹) |
|-----------------------|---------------|-----------------------------|---------------------------------|------|-----------------------------|------------------------------|---|
| 2022 | | | | | | | |
| Mean | 8.7 | 11.59 | 188 | 7.03 | 0.648 | 0.06 | 0.00467 |
| Min | 6.4 | 8.69 | 135 | 5.65 | 0.100 | 0.06 | 0.00326 |
| Max | 16.1 | 12.95 | 267 | 9.15 | 4.333 | 0.10 | 0.02391 |
| E1 mean | 7.6 | 12.47 | 188 | 7.02 | 0.767 | 0.06 | 0.00568 |
| E2 mean | 9.1 | 11.94 | 197 | 7.03 | 0.611 | 0.06 | 0.00414 |
| E3 mean | 9.6 | 10.48 | 177 | 7.05 | 0.515 | 0.06 | 0.00351 |
| 2018 | | | | | | | |
| Mean | 9.4 | 10.95 | 153 | 7.35 | - | - | - |
| Min | 6.8 | 8.56 | 101 | 5.99 | - | - | - |
| Max | 15.8 | 12.64 | 292 | 9.21 | - | - | - |
| 2006 (plateau) | | | | | | | |
| Mean | 6.4 | 11.59 | 192 | 6.92 | 0.047 | 0.00564 | 0.0070 |
| Min | 5.5 | 11.35 | 164 | 6.35 | 0.003 | 0.00004 | 0.0013 |
| Max | 7.4 | 11.80 | 224 | 7.46 | 0.092 | 0.02449 | 0.0155 |
| 2006 (coastal) | | | | | | | |
| Mean | 8.4 | 11.32 | 889 | 7.19 | 0.719 | 1.23331 | 1.124 |
| Min | 6.0 | 9.17 | 406 | 5.50 | 0.074 | 0.02430 | 0.007 |
| Max | 13.1 | 14.43 | 1482 | 8.13 | 2.706 | 9.89000 | 4.636 |

291
 292 Table 2: Mean major ions (mmol L⁻¹) and stable water isotope (‰) results for the 40 lakes sampled in 2018 and 2022.

| | Cl | SO_4 | Br | Na | Ca | Mg | K | SiO_2 | Fe | F- | Al | $\delta^{2\text{H}}$ | $\delta^{18\text{O}}$ |
|-------------|-------|---------------|-------|-------|-------|-------|-------|----------------|-------|-------|-------|----------------------|-----------------------|
| 2018 | | | | | | | | | | | | | |
| Mean | 1.965 | 0.103 | 0.003 | 1.350 | 0.085 | 0.325 | 0.032 | 0.013 | 0.001 | 0.001 | 0.002 | -20.1 | -2.8 |
| Min | 1.379 | 0.065 | 0.001 | 0.987 | 0.025 | 0.219 | 0.005 | 0.001 | 0.000 | 0.001 | 0.000 | -34.9 | -5.3 |
| Max | 3.667 | 0.211 | 0.007 | 2.566 | 0.287 | 0.590 | 0.064 | 0.087 | 0.003 | 0.006 | 0.006 | -1.9 | 0.7 |
| 2022 | | | | | | | | | | | | | |
| Mean | 1.593 | 0.083 | 0.002 | 1.272 | 0.080 | 0.197 | 0.029 | 0.020 | 0.001 | 0.002 | 0.002 | -23.4 | -3.3 |
| Min | 1.191 | 0.055 | 0.001 | 0.931 | 0.025 | 0.133 | 0.009 | 0.003 | 0.000 | 0.000 | 0.000 | -35.6 | -5.3 |
| Max | 2.779 | 0.155 | 0.005 | 2.073 | 0.289 | 0.369 | 0.052 | 0.130 | 0.011 | 0.021 | 0.022 | -14.6 | -1.7 |
| E2 Mean | 1.426 | 0.076 | 0.002 | 1.229 | 0.079 | 0.150 | 0.028 | 0.027 | 0.001 | 0.003 | 0.003 | -30.1 | -4.6 |
| E3 Mean | 1.436 | 0.075 | 0.002 | 1.228 | 0.081 | 0.150 | 0.027 | 0.022 | 0.001 | 0.002 | 0.002 | -23.4 | -3.2 |
| E4 Mean | 1.448 | 0.073 | 0.002 | 1.223 | 0.075 | 0.146 | 0.026 | 0.018 | 0.001 | 0.002 | 0.002 | -20.7 | -2.8 |



293



294

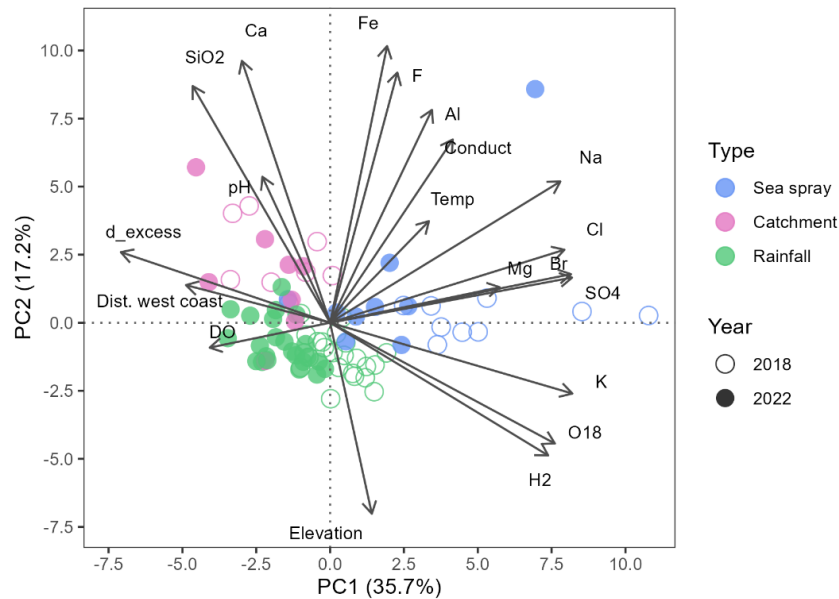
295 **Figure 3:** Scholler plot comparing the ionic composition (SO_4 , Cl, Mg, Na, K, Ca, F and SiO_2) of Macquarie Island lake waters and
296 seawater (red line), categorised into sampling years 2018 (black lines) and 2022 (grey lines).

297 Statistical analysis showed almost no significant differences in major ion concentrations across 2022
298 sampling events (E2–4), with the only significant difference occurring in Br between E2 and E4 ($p =$
299 0.023). Broader changes were detected between 2018 and 2022, with Cl, SO_4 , Br, and Mg all showing
300 higher mean concentrations in 2018 compared to all 2022 sampling events (E2–4). K and SiO_2 were
301 greater in E1 in comparison to E4 and E2–3, respectively. Fe, Na, Ca, F, and Al did not significantly vary
302 ($p > 0.05$) between sampling events. All ions that show significant variation ($p < 0.05$) have predominantly
303 marine sources.

304 PCA showed the relationship between lake water chemistry parameters, with samples grouped by lake
305 type and sampling year (Fig. 4). Together, PC1 and PC2 captured 53% of the total variance in the
306 dataset. PC1 represents a salinity and sea-spray gradient with variability in EC, distance from the west
307 coast, Na, Cl, Br, Ca, Mg, and K captured. PC2 represents an altitude and terrestrial ion gradient with
308 variability in elevation, temperature, SiO_2 , Ca, Fe, and F captured. Lakes cluster according to
309 environmental processes (groups derived from Meredith et al., 2022), with SSA influenced lakes having
310 positive PC1 scores, which suggests higher concentrations of marine derived ions. Three sea spray
311 influenced outliers can be seen across PC1: LK3 in 2018 and LK37 in both 2018 and 2022. The grouping
312 of samples influenced by catchment processes and those influenced by rainfall is driven by PC2 with
313 catchment influence lakes having lower elevation and higher ion concentrations. SSA and rainfall



314 influenced lakes cluster based on the year that they were sampled with greater ion concentrations in
315 2018.



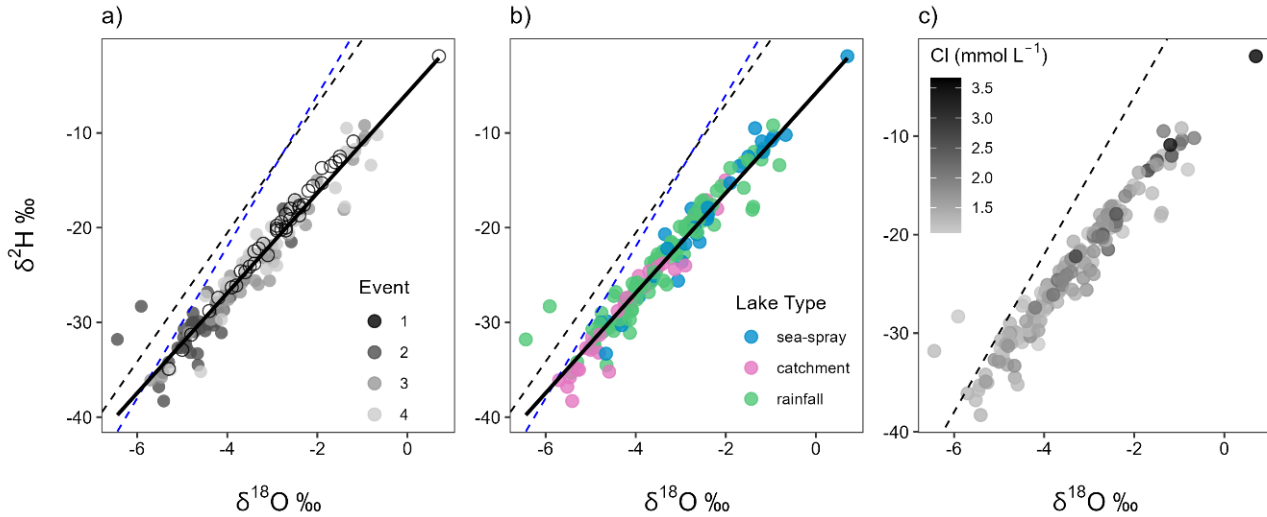
316

317 **Figure 4: Principal Component Analysis (PCA) of Macquarie Island lake waters, showing the relationships between major ions and**
318 **environmental parameters. Lakes are coloured by lake type, showing that lakes cluster based on the dominate geochemical**
319 **processes identified by Meredith et al., (2022). Dist. west coast = distance from the west coast (m), Conduct = electrical conductivity.**

320 3.2 Stable water isotopes

321 The $\delta^{2\text{H}}$ and $\delta^{18\text{O}}$ values were measured in the 2022 samples and ranged from -38.3‰ to -9.2‰ and -38.3‰ to -0.67‰ , respectively. Lake waters in 2018 and 2022 fell below the Global and Cape Grim
322 (northwest Tasmania) Meteoric Water Lines (MWLs), suggesting slight isotopic enrichment in Macquarie
323 Island's lakes (Fig. 5). In 2018 lake waters were significantly higher in $\delta^{2\text{H}}$ (mean -24.8‰) and $\delta^{18\text{O}}$
324 (mean -2.83‰) compared to 2022 (mean $\delta^{2\text{H}} = -24.8\text{‰}$ and $\delta^{18\text{O}} = -3.55\text{‰}$). Significant isotopic
325 enrichment of $\delta^{2\text{H}}$ and $\delta^{18\text{O}}$ ($p < 0.001$) can be seen in the data at the beginning of the 2022 austral
326 summer (E2–3; Fig. 5a). SSA influenced lakes tended to have higher isotopic values, while catchment
327 influenced lakes had lower values (Fig. 5b), with a significant difference between all lake types detected
328 ($p < 0.001$). LK20 and LK21 from E2 were outliers, plotting above the MWLs with lower $\delta^{18\text{O}}$ values. Cl
329 concentrations appeared to be related to $\delta^{2\text{H}}$ and $\delta^{18\text{O}}$ values (Fig. 5c), however the correlation between
330

331 the parameters was low ($r^2 \leq 0.24$). This lack of relationship was consistent across lake types and
332 sampling events.



333
334 Figure 5: Stable water isotope $\delta^{2\text{H}}$ and $\delta^{18\text{O}}$ differences in Macquarie Island lake waters, shown across: a) sampling events; b) lake
335 type; c) $\delta^{2\text{H}}$ and $\delta^{18\text{O}}$ relationship shown with Cl concentration (mmol L^{-1}). Solid black line show Macquarie Island regression, blue
336 dashed line is the global meteoric water line (GMWL: $\delta^{2\text{H}} = 8 \delta^{18\text{O}} + 10$), and black dashed line is the Cape Grim local meteoric water
337 line (LMWL: $\delta^{2\text{H}} = 6.8 \delta^{18\text{O}} + 6.65$).

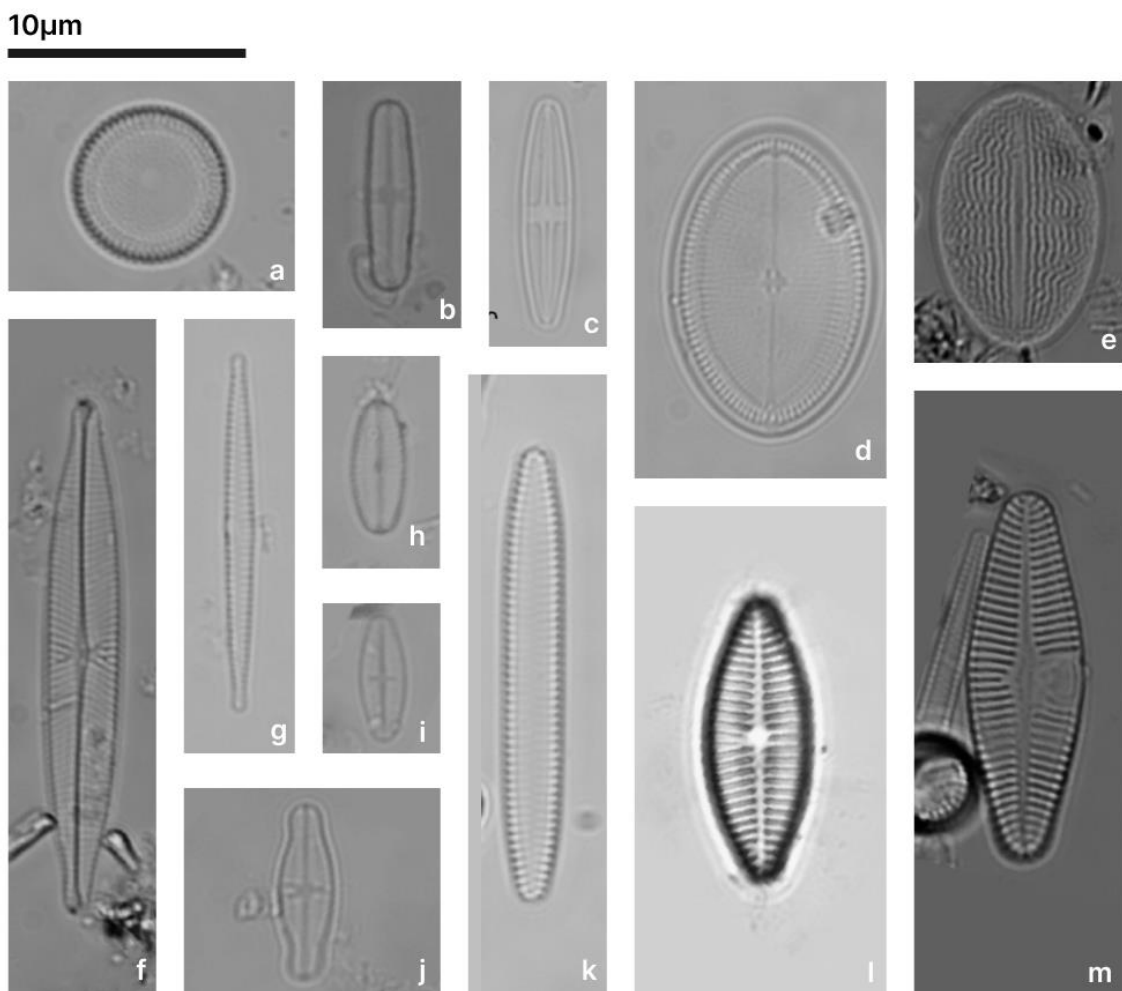
338 3.3 Diatoms

339 3.3.1 Diatom communities

340 In total 141 diatom taxa from 45 genera were identified in the 52 plateau and coastal lakes. Ninety-six
341 taxa from 30 genera remained in the dataset after taxa with < 1% relative abundance were excluded.
342 The most taxon-rich genera were *Pinnularia* (16 taxa), *Psammothidium* (12 taxa), and *Planothidium* (8
343 taxa). The most dominant taxa being both common, occurring in > 15 lakes, and abundant, occurring >
344 25% relative abundance in at least one sample, were *Aulacoseira principissa* Van de Vijver,
345 *Psammothidium abundans* (Manguin) Bukhtiyarova & Round, *Psammothidium confusum* var. *atomoides*
346 (Manguin) van de Vijver, unknown species 111, *Psammothidium confusum* (Manguin) van de Vijver,
347 *Fragilaria capucina* Desmazières, and *Navicula bergstromiana* Vyverman et al. Coastal and plateau
348 lakes showed distinctly different assemblages, with coastal lakes exhibiting less diversity (mean number
349 of species = 20) and dominated by taxa including *F. capucina*, unknown sp. 111, *Planothidium*
350 *quadripunctatum* (D.R.Oppenheim) Sabbe, *Planothidium delicatum* (Kützing) Round & Bukhtiyarova,
351 and *Planothidium lanceolatum* (Brébisson ex Kützing) Lange-Bertalot. Plateau lakes were more diverse
352 (mean number of taxa = 40) and dominated by *A. principissa*, *P. abundans*, *P. confusum* var. *atomoides*,



353 *P. confusum*, and *N. bergstromiana*, *Achnanthidium modestiformis* (Lange-Bertalot) Van de Vijver,
354 *Cocconeis placentulata* Ehrenberg, and unknown species 21. No taxa were found in all lakes. See Figure
355 6 for microscopy photos of the most abundant taxa.



356
357 Figure 6: The most abundant diatom taxa from plateau and coastal lakes on Macquarie Island. a) *Aulacoseira principissa*, b)
358 *Psammothidium abundans*, c) *Psammothidium confusum*, d-e) *Cocconeis placentulata*, f) *Navicula bergstromiana*, g) *Fragilaria*
359 *capucina*, h) unknown species 21, i) *Psammothidium confusum* var. *atomoides*, j) *Achnanthidium modestiformis*, k) unknown species
360 111, l) *Planothidium delicatulum*, m) *Planothidium lanceolatum*.

361 3.3.2 Diatom-environment relationships

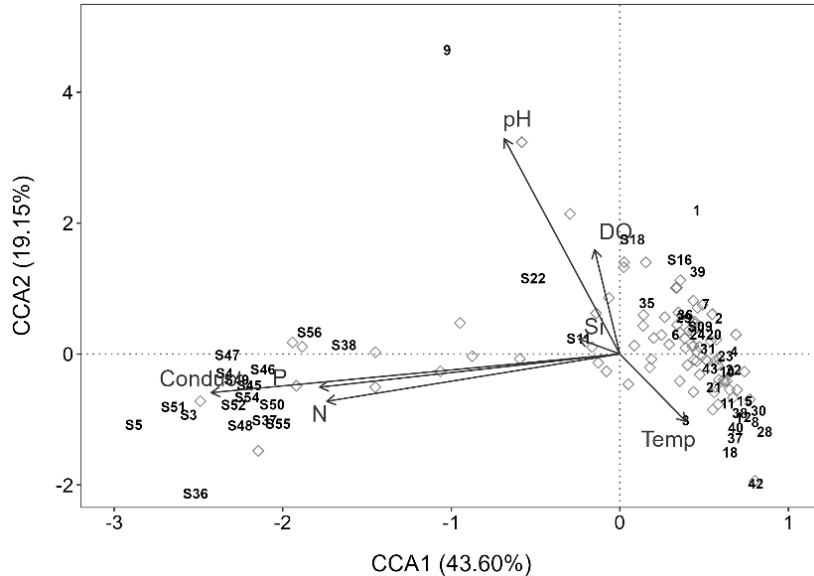
362 The full CCA model was significant ($p = 0.001$), with environmental variables explaining 23.9% (Table 3)
363 of the total variance in diatom species composition (constrained inertia = 1.5). Together, the first two
364 canonical axes explained 62.8% of the total constrained variance (Table 3; Fig. 7). Forward selection



365 identified EC, pH, and temperature as the most significant predictors of diatom community composition
366 ($p = 0.001$), collectively explaining 15.4 % of the total variance. This equates to 70% of the total explained
367 variance in the full model, capturing the major environmental gradients influencing species distribution
368 with a more parsimonious model.

369 **Table 3: Full CCA model results**

| Axis | Eigenvalue | Proportion of variance explained (%) | Cumulative proportion (%) |
|----------------------------|------------|--------------------------------------|---------------------------|
| CCA1 | 0.67 | 43.60 | 43.60 |
| CCA2 | 0.30 | 19.15 | 62.75 |
| CCA3 | 0.21 | 13.36 | 76.11 |
| CCA4 | 0.15 | 7.61 | 85.60 |
| Constrained inertia | 1.5 | | |
| Constrained proportion (%) | 23.97 | | |



370
371 **Figure 7: Full CCA ordination biplot of diatom species and environmental data, numbers indicate sites, and grey symbols indicate**
372 **diatom species. Si = silicate, P = phosphate, N = total oxidised nitrogen, and conduct = electrical conductivity.**

373 Individual CCAs were performed to assess the total explanatory power of each variable. EC and pH were
374 shown to be the strongest, individually explaining 10.03% and 4.56% of the total variation, respectively.
375 This corresponds to 45.83% and 20.86% of the total variance in the full CCA model. Additionally, EC
376 was the only variable with a high λ_1/λ_2 ratio ($\lambda_1/\lambda_2 = 1.31$; Table 4), suggesting it is the only variable with
377 enough explanatory power for inference modelling.



378

Table 4: Individual CCA results, independent CCAs run for each variable. (* = significant p value < 0.05)

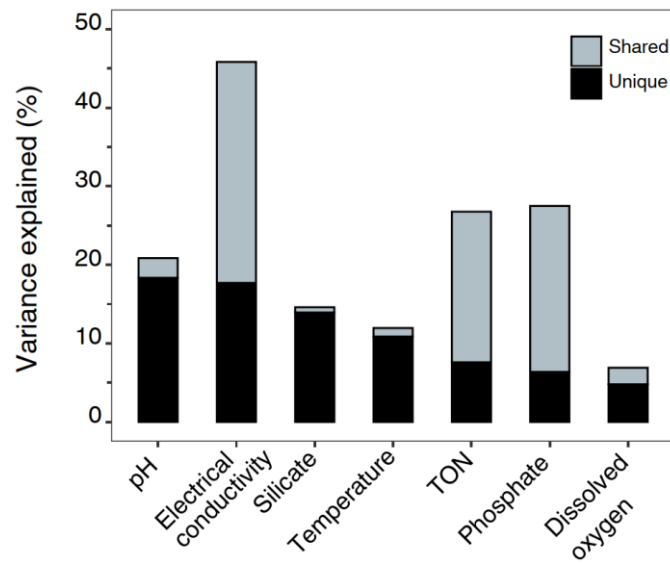
| Variable | λ_1 / λ_2 | Constrained sum | Variance explained (%) | Proportion of full model explained (%) | p-value |
|-------------------------|-------------------------|-----------------|------------------------|--|---------|
| Electrical conductivity | 1.31 | 0.64 | 10.03 | 45.83 | 0.001* |
| Phosphate | 0.73 | 0.38 | 6.02 | 27.5 | 0.001* |
| Total oxidised nitrogen | 0.68 | 0.37 | 5.86 | 26.78 | 0.001* |
| pH | 0.39 | 0.29 | 4.56 | 20.86 | 0.001* |
| Silicate | 0.26 | 0.20 | 3.2 | 14.61 | 0.023* |
| Temperature | 0.22 | 0.17 | 2.62 | 11.96 | 0.176 |
| Dissolved oxygen | 0.12 | 0.10 | 1.51 | 6.9 | 0.879 |

379

380 Partial CCAs were performed with each environmental variable tested separately while controlling for
 381 covariation with all other variables, to quantify unique and shared variance contributions. EC, pH, and Si
 382 were the only variables to have significant unique contributions ($p \leq 0.01$; Partial CCA Table 5). The shared
 383 and unique variance of each environmental variable is shown in Figure 8. EC explained the largest
 384 proportion of total constrained variation (46%) in diatom community composition, with a large shared
 385 component (17% unique, 28% shared), suggesting it acts along a major environmental gradient shared
 386 with TON and PO_4^{3-} (Fig. 8). Despite this, it performed well in all other CCAs and its unique contribution
 387 remained high, indicating it is an important independent driver of diatom structure across Macquarie
 388 Island lakes. Furthermore, low VIFs among all environmental variables (VIFs < 3) indicated that
 389 multicollinearity was low. EC (VIF = 2.6) showed a low correlation with other variables ($r^2 \leq 0.47$),
 390 suggesting it represents a largely independent gradient in the dataset. In contrast, pH had similar unique
 391 variance (18.4%) and lower shared variance (2.4%), implying a more independent ecological influence.
 392

393 **Table 5: Partial CCA results, where each variable was tested with the covariation of other variables controlled (* = significant p value < 0.05).**

| Variable | Variance explained (%) | Proportion of full model explained (%) | p-value |
|-------------------------|------------------------|--|---------|
| pH | 5.02 | 18.35 | 0.002* |
| Electrical conductivity | 4.85 | 17.7 | 0.001* |
| Silicate | 3.85 | 13.93 | 0.013* |
| Temperature | 3.03 | 10.87 | 0.151 |
| Total oxidised nitrogen | 2.14 | 7.6 | 0.651 |
| Phosphate | 1.8 | 6.37 | 0.774 |
| Dissolved oxygen | 1.36 | 4.8 | 0.991 |



394

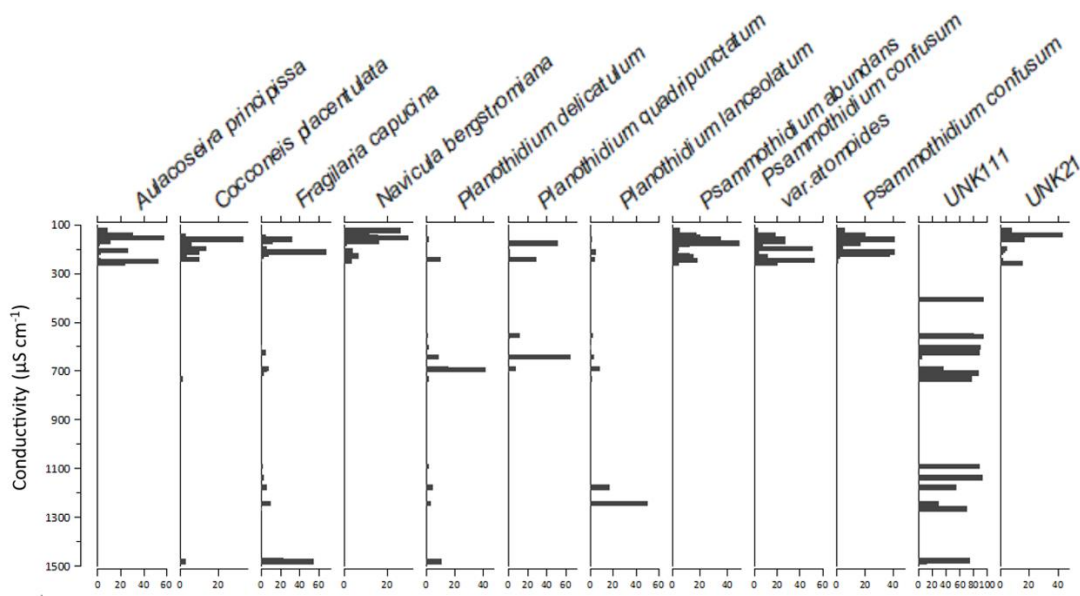
395 Fig. 8: Variance partitioning showing unique and shared proportions of variance explained by each environmental variable.

396 3.3.3 Species optima and tolerances

397 Species optima and tolerance across major environmental gradients EC, pH, and temperature were
398 determined with WA. *F. capucina*, *P. lancelotum*, and *P. delicatulum* were found across the EC range,
399 however each species showed different optima (Fig. 9). Unknown sp. 111 was found to tolerate mid to
400 high-level EC, while most other dominant species, including *A. principissa*, *C. placentulata*, *N.*
401 *bergstromiana* and dominant *Psammothidium* species have highest abundance at low EC sites.

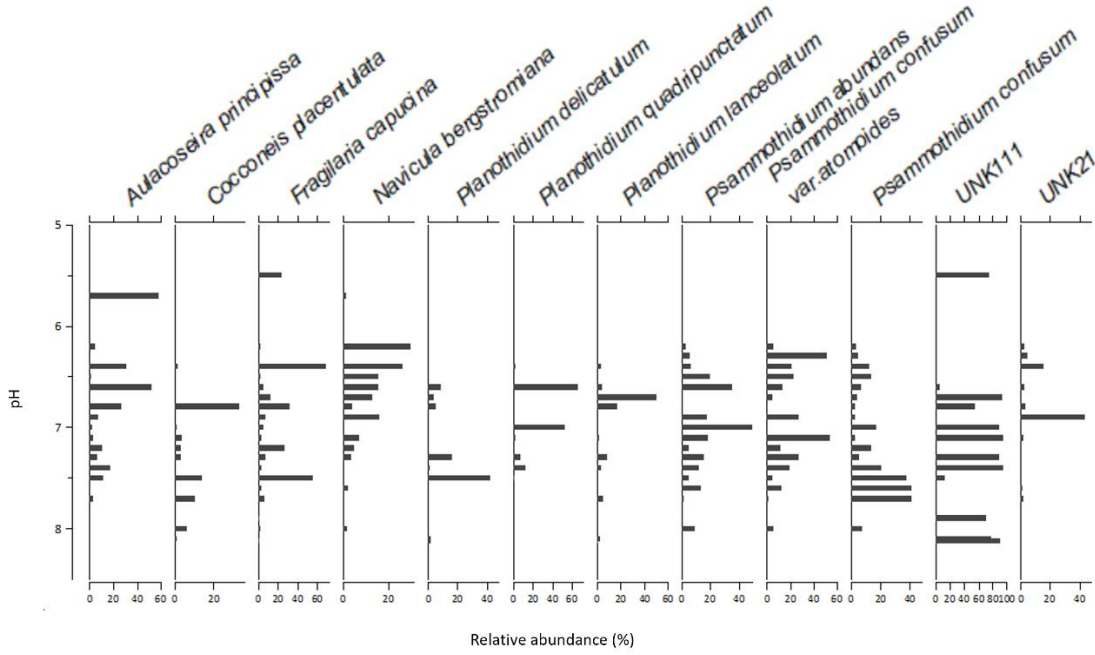
402

403 Species optima were less clear for pH, as the dominant species had tolerances across the pH gradient,
404 ranging from slightly acidic to slightly alkaline (Fig. 10). *A. principissa*, *N. bergstromiana*, and *P.*
405 *confusum* var. *atomoides* showed optima for slightly acidic sites. While *P. confusum* had higher
406 abundances at slightly alkaline sites. *C. placentulata*, *P. lanceolatum*, *P. quadripunctatum*, and unknown
407 sp. 21 showed preferences for neutral pH, and unknown sp. 111 for neutral to slightly acidic sites.
408 Species optima for temperature are described in Supplementary Material Figure S1.



409

410 **Figure 9: Relative abundance of the most dominant diatom species along the conductivity gradient (126–1482 µS/cm), UNK = unknown**
411 **species.**



412

413 **Figure 10: Relative abundance of the most dominant diatom species along the pH gradient (5.50–9.14 °C), UNK = unknown species.**



414 3.3.4 Diatom transfer functions

415 Ordination analyses showed that EC and pH explained significant and independent proportions of
416 variance in diatom composition, with temperature contributing to a lesser extent. As such, transfer
417 functions were developed for each. While Si was shown to independently contribute to diatom variance,
418 reduced CCA modelling with forward selection did not indicate it to be a major environmental gradient.
419 Transfer function results for the best performing WA, WAPLS, or ML model for each environmental
420 variable are described in Table 6.

421

422 **Table 6: Best performing WA, WAPLS or ML model results for conductivity, pH, and temperature.**

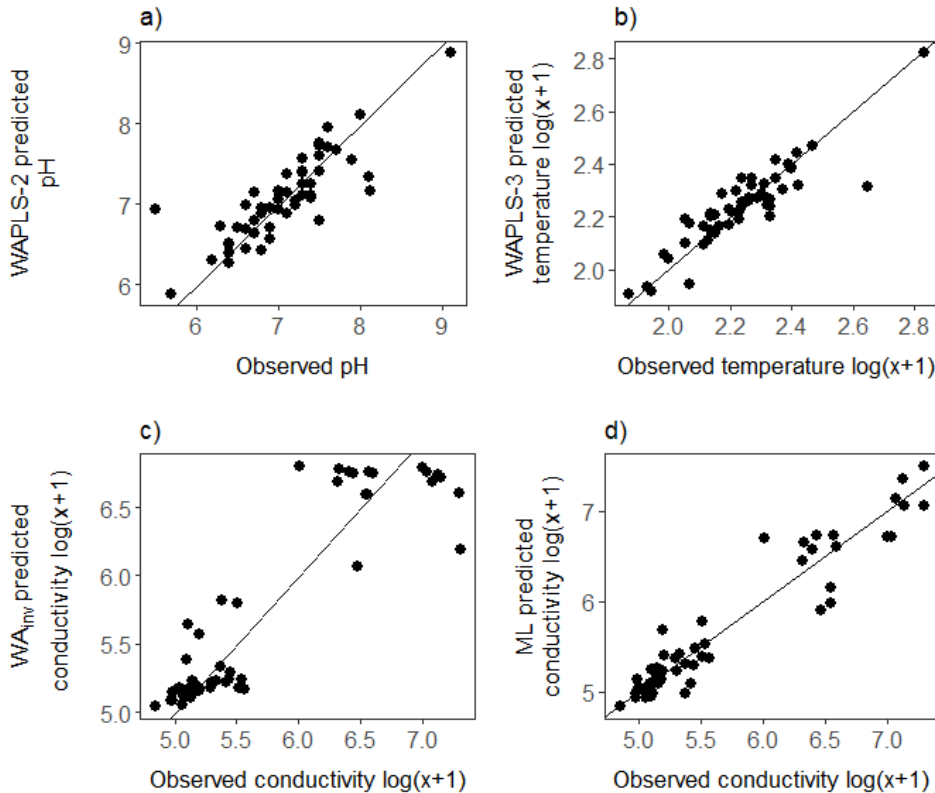
| Variable | Model | r^2 | r_{boot}^2 | RMSE | RMSEP |
|-------------------------|-------------------|-------|--------------|------|-------|
| Electrical conductivity | WA _{inv} | 0.83 | 0.74 | 0.31 | 0.39 |
| | ML | 0.91 | 0.80 | 0.22 | 0.40 |
| pH | WAPLS-2 | 0.69 | 0.17 | 0.34 | 0.63 |
| Temperature | WAPLS-3 | 0.81 | 0.19 | 0.07 | 0.18 |

423

424 For EC, WA_{inv} and WAPLS-1 produced near identical results. WA_{inv} was favoured as the simpler model
425 (WA_{inv}, $r^2 = 0.83$, $r_{boot}^2 = 0.74$, RMSE = 0.31, RMSEP = 0.39). Although WAPLS-2 to -5 increased r^2 and
426 reduced RMSE, each successive component progressively increased RMSEP by 13-16%, thereby
427 reducing performance. Given the unimodal gradient structure of the dataset, ML modelling was also
428 assessed for EC. ML showed slightly stronger predictive performance to WA_{inv}, with higher r_{boot}^2 and
429 comparable RMSEP (ML, $r^2 = 0.91$, $r_{boot}^2 = 0.80$, RMSE = 0.23, RMSEP = 0.40).

430

431 Comparison of observed and predicted value scatter plots indicated that ML achieved a tighter fit, with
432 WA_{inv} showing increased predictive error at higher EC ranges (Fig. 11). However, further inspection
433 indicated that only ~30% of taxa displayed Gaussian (Type IV–V) response curves indicating ML may
434 not be the most appropriate approach (see Supplementary Figure S2 and Table S4 for full Gaussian
435 response curve results). However, overfitting from ML is not likely as RMSEP did not increase. Overall,
436 both models show cross-validated performance and are considered robust.



437

438 **Figure 11: Comparison of observed environmental measurements with values predicted by diatom-based transfer functions: a) pH**
439 **estimated using WAPLS-2; b) temperature estimated using WAPLS-3; c) conductivity estimated using WA with inverse deshrinking**
440 **(WA_{inv}); and d) conductivity estimated using the modern analogue (ML) method. Black lines show the 1:1 line.**

441

442 pH had poor performance across all WA and WAPLS models with high RMSEP (> 0.6) and low r_{boot}^2 (≤ 0.2). WAPLS-2 was found to be the strongest model (WAPL-2, $r^2 = 0.69$, $r_{boot}^2 = 0.17$, RMSE = 0.34, RMSEP = 0.63). Temperature had similarly low r_{boot}^2 (< 1.9) across models but low RMSEP (≤ 0.2) with WAPLS-3 showing the best performance (WAPLS-3, $r^2 = 0.81$, $r_{boot}^2 = 0.19$, RMSE = 0.07, RMSEP = 0.18). ML modelling showed poor performance for pH with high RMSEP = 0.93 and temperature with low $r_{boot}^2 = 0.08$.



448 4 Discussion

449 4.1 Annual and seasonal lake water hydrogeochemical variation

450 The seasonal hydrochemistry dataset presented in this study support the 2018 baseline assessment
451 (Meredith et al., 2022) that lake water chemistry is controlled by SSAs, terrestrial catchment processes,
452 elevation and rainfall dilution.

453

454 The seasonal water chemistry data, which is presented for the first time in this study, shows that there
455 is little to no significant variation in major ions across the 2022–23 austral summer. Variations in Br were
456 observed but can be explained as being related to localised sources associated with increased organic
457 inputs from runoff rather than SSA sources. This is indicated by Cl/Br ratios generally falling below the
458 seawater line (Supplementary Fig. S3), suggesting Br has additional non marine sources. Br is known
459 to be enriched in dissolved and particulate organic matter and mobilised during catchment run-off events,
460 particularly in peat-dominated sub-Antarctic landscapes (Gerritse & George, 1988; Biester et al., 2004;
461 Guevara et al., 2019). This interpretation is further supported by differing monthly rainfall amounts for
462 Macquarie Island, where higher mean monthly rainfall occurred during E3 (January - 98 mm) and E4
463 (February -93 mm) compared to E2 (December -59 mm; BOM, 2025).

464

465 A comparison of 2018 and 2022 data shows that significant variation ($p < 0.05$), in some major ions is
466 evident, with higher concentrations in 2018 of Br and Cl, SO_4 , and Mg associated with SSAs. Although
467 not statistically significant ($p > 0.05$), other sea-spray derived ion mean values (Na, Ca, K) were higher
468 in 2018 (Table 2). However not all ions increased in concentration. In particular, terrestrial derived ions
469 such as Fe, F, Si, and Al were lower in 2018. This suggests that lakes in 2022 had a stronger SSA
470 influence.

471

472 Despite these changes, PCA of the 2018 and 2022 lake water chemistry datasets (Fig. 4) show that
473 lakes typically cluster by the lake types identified in Meredith et al. (2022) (i.e., as SSA, catchment and
474 rainfall influenced). This indicates that the major hydrogeochemical processes influencing Macquarie
475 Island lakes are consistent between years, with no major environmental shifts occurring in weathering
476 and erosion of the island's geology, suggesting these processes are stable on an annual time scale.
477 Identifying hydrogeochemical stability is important for identifying lake sites suitable for diatom-



478 conductivity inference models. It also strengthens palaeoclimate interpretations by suggesting that local
479 lake dynamics are relatively constant, supporting the hypothesis that in sea-spray dominated lakes,
480 proxies primarily record externally forced changes driven by the SHW rather than internal hydrological
481 or geochemical dynamics (Saunders et al., 2018; Perren et al., 2020). This further emphasises that water
482 chemistry characteristics are critical to consider in site-selection, to develop reliable SHW
483 reconstructions on Macquarie Island.

484

485 Furthermore, the development of the transfer function using field parameters collected across multiple
486 sampling events increases confidence that the model reflects representative environmental conditions
487 (Goldenberg Vilar et al., 2018; Kennedy & Buckley, 2021). This repeated-sampling approach is rarely
488 possible when constructing diatom transfer functions, particularly in remote regions like the sub-Antarctic
489 and Antarctic. While this adds robustness to the diatom model developed here, the data does not include
490 winter measurements. The transfer functions could therefore be improved with year-round lake
491 monitoring to capture the full range of environmental variability.

492 **4.2 Evaporation**

493 Interpreting environmental proxies as direct indicators of climate variability can be challenging, as
494 multiple processes may produce similar signals (Molén, 2024). When using diatom–conductivity models
495 to infer past SHW variability, it is essential to consider how near surface evaporation has the potential to
496 concentrate ions in surface waters and mimic the effects of other processes such as increasing lake
497 water salinity from SSA deposition due to stronger winds. Although this study and previous studies
498 (Evans, 1970; Buckney & Tyler, 1974; Meredith et al., 2022) have demonstrated that SHW-driven SSA
499 inputs are a dominant control on lake water chemistry on Macquarie Island, the role of evaporation in
500 amplifying these signals remains unclear.

501

502 To explore this, we analysed $\delta^{2\text{H}}$ and $\delta^{18\text{O}}$ values from 2018 and across the 2022–23 summer. Isotopic
503 enrichment is evident across the 2022–23 season (Fig. 5a), unsurprisingly indicating a strengthening
504 evaporative signal through summer. Lake stable water isotopes sampled in 2018 were significantly more
505 enriched than the 2022 mean, as expected given that the 2018 samples were collected in late summer,
506 when evaporative effects are strongest and cumulative due to warmer temperatures throughout summer.
507 This is supported by lake water temperatures being significantly lower in early summer (E2) compared



508 to late summer (E3 and E4; Table 1). Given Macquarie Island's persistently high cloud cover, humidity,
509 and low sunshine hours (BOM, 2025), solar evaporation is likely limited and confined to the summer
510 season. Evaporation can produce heavy-isotope enrichment and the residual lake water becomes
511 progressively enriched in heavier isotopes ($\delta^2\text{H}$ and $\delta^{18}\text{O}$), moving away from the Global MWL (Gat, 1996).
512 Comparisons between E1 (2018) and E4 (2022), which were sampled at the same time of the year in
513 January–February provide a valuable comparison of potential interannual variability in lake water
514 chemistry and processes (Table 2). These two sampling events show near identical mean isotopic
515 composition ($p > 0.05$; $\delta^2\text{H} = -20.7\text{\textperthousand}$ and $\delta^{18}\text{O} = -2.8\text{\textperthousand}$ in 2022, and $\delta^2\text{H} = -20.1\text{\textperthousand}$ and $\delta^{18}\text{O} = -2.8\text{\textperthousand}$
516 in 2018), suggesting broadly stable summer evaporative conditions between years. Furthermore, SSA
517 influenced lakes on the plateau are in proximity to the west coast and have the greatest exposure to the
518 SHW (Fig. 2b). These lakes have significantly higher isotopic enrichment (Fig. 5b), providing further
519 evidence that wind is likely the primary driver of evaporation in plateau lake waters across Macquarie
520 Island, particularly in lakes located on the western coast, which may be most suitable for reconstructions
521 of SHW dynamics. As both wind-enhanced evaporation and wind-driven SSA transport and deposition
522 contributes to the concentration of SSA ions in these lakes, both ion deposition and the concentration
523 reflect a SHW signal.

524

525 Cl^- is a robust tracer of hydrogeochemical processes and, together with $\delta^2\text{H}$ and $\delta^{18}\text{O}$ values, can be
526 used to better understand evaporation (Kirchner et al., 2010). While the isotopic enrichment observed
527 generally indicates an evaporative signal, the absence of a correlation between Cl^- and $\delta^2\text{H}$ or $\delta^{18}\text{O}$
528 suggests that isotopes are capturing short-term (summer) evaporation rather than sustained evaporative
529 concentration sufficient to increase Cl^- concentration in the lake waters like those in environments driven
530 primarily by solar evaporation (Meredith et al., 2009). On Macquarie Island, wind-driven SSA deposition
531 and rainfall dilution therefore likely remain the primary drivers of Cl^- variability. Consequently, EC in lake
532 waters of Macquarie Island remains a robust proxy for interpreting variations in SHW strength.

533 4.3 Diatom communities

534 Diatom analysis showed that typical sub-Antarctic genera (Van de Vijver, 2019; Goeyers et al., 2022),
535 including *Psammothidium*, *Planothidium*, and *Fragilaria*, dominated lake diatom communities on
536 Macquarie Island. Across 52 lakes, 141 taxa were identified, indicating intermediate species diversity
537 relative to previous studies on the island which reported 102 (McBride, 2009) and 208 (Saunders et al.,



538 2009) species. Consistent with these earlier studies we have demonstrated that diatoms on Macquarie
539 Island exhibit clear and distinct ecological preferences. Combined with the pronounced environmental
540 gradients among lakes, these species-environment relationships provide a strong basis for using diatoms
541 as indicators of limnological conditions and environmental change.

542

543 *Psammothidium* species are characteristic of low EC sites (Van de Vijer et al., 2002), and while
544 abundance and dominance of key *Psammothidium* species showed variation along the lower end of the
545 EC gradient, they dominated low EC sites. *N. bergstromiana* is considered endemic to Macquarie Island
546 and was commonly found with dominant *Psammothidium* species at low EC sites, typically occurring
547 where EC was $< 200 \mu\text{S cm}^{-1}$, consistent with what has previously been reported (Sabbe et al., 2019).
548 *A. principissa*, previously identified as *Aulacoseria distans* (Ehrenberg) Simonsen on Macquarie Island
549 (McBride, 2009; Saunders et al., 2009), was also common at low EC. This taxa is commonly found on
550 sub-Antarctic Islands and is suggested to prefer very low conductance values $< 80 \mu\text{S cm}^{-1}$ (Van de
551 Vijver, 2012), while EC was not observed $< 160 \mu\text{S cm}^{-1}$ in this dataset, *A. principissa* may be an indicator
552 of very low EC conditions.

553

554 *P. lanceolatum* was a dominant high EC, high nutrient taxa. While it has been found to dominate flora
555 elsewhere, this contrasts previous studies where it has been reported to be characteristic of oligotrophic
556 conditions (Van de Vijer et al., 2002). *F. capucina*, *P. delicatulum*, and unknown sp. 111 were more
557 commonly dominant at high EC. *F. capucina* was found across the EC gradient, consistent with its
558 cosmopolitan and ecologically tolerant nature (Van de Vijer et al., 2002).

559 **4.4 Developing transfer functions**

560 A key aim of this study was to update and improve existing quantitative diatom models for Macquarie
561 Island. While the dominant taxa identified here are consistent with those reported by Saunders et al.
562 (2009), the strength of some diatom–environment relationships differ. EC and pH remain strong
563 explanatory variables for diatom variation, whereas PO_4^{3-} and Si showed limited influence in this study.
564 This reduced explanatory power likely reflects the low nutrient variability across plateau lakes, where
565 concentrations were generally below detection limits.

566



567 Sub-Antarctic lakes are characteristically oligotrophic; high nutrient levels do occur, but they are
568 associated with peatlands or animal colonies, as is the case with coastal lakes on Macquarie Island
569 (Selkirk et al., 1990). The Saunders et al. (2009) dataset recorded greater nutrient variability across
570 plateau sites at the lower end of the EC gradient, attributed to enhanced organic inputs during periods
571 of high ecological disturbance from invasive rabbits. These differences suggest that the dataset in this
572 study better represents post-invasive or recovered limnological conditions that more likely reflect pre-
573 invasion or baseline states and provides an updated basis for developing robust diatom–environment
574 models.

575

576 EC was shown to be the major independent driver of diatom assemblages, with strong performance in
577 all CCA models, individually accounting for almost 50% of the variance in the full CCA model and strong
578 explanatory power as indicated by λ_1/λ_2 (Table 4). Although EC reflects a high proportion of shared
579 variance (Fig. 8), this is consistent with its role as an integrative measure of ionic strength and catchment
580 inputs. The shared component primarily reflects its covariation with major ions and nutrient variables
581 (TON and PO_4^{3-}), which are typically correlated with EC in these systems. Despite this overlap, EC
582 retained a strong and highly significant independent effect ($p = 0.001$), confirming its dominant ecological
583 influence on diatom distributions.

584

585 While PO_4^{3-} , TON, and Si each explained significant but moderate portions of individual variance (Table
586 4), they lost significance once covariation was controlled for (Table 5), meaning their explanatory power
587 is mostly shared variance with other environmental gradients, primarily EC and each other. While pH
588 explained a major and independent gradient in diatom variation within plateau lakes (Fig. 7), it did not
589 capture assemblage changes across high-EC, high-nutrient sites. This was indicated by individual CCA
590 results, which were less than half of the variance explained by EC (Table 4). This, paired with the
591 widespread oligotrophic nature of plateau lakes on Macquarie Island lends strength to the explanatory
592 power of EC across the whole dataset.

593

594 Furthermore, pH showed poor predictive performance as a transfer function, with the lowest $r_{boot}^2 = 0.17$,
595 and highest RMSEP = 0.63 from the WAPLS-2 model. While this is surprising due to the strong pH
596 gradient across plateau sites, most diatoms were tolerant across the pH gradient with few species
597 showing clear optima for narrowed and specific ranges. EC had the strongest performance with the WA



598 and ML models producing the highest r_{boot}^2 (0.74 and 0.80, respectively) and comparable RMSEP. WA_{inv}
599 and WAPLS-1 showed identical performance, with no benefit from additional WAPLS components, which
600 progressively increased predictive error and decreased r_{boot}^2 , suggesting overfitting. WA was therefore
601 chosen over WAPLS as the simpler model.

602

603 The WA EC transfer function performed better than the previously published Macquarie Island diatom-
604 conductivity transfer function (Saunders et al., 2009), with higher r_{boot}^2 . However, some caution is
605 warranted when predicting across the upper EC range, where greater predictive error is evident (Fig.
606 11). This can be attributed to lower species turnover, higher variability in PO₄³⁻, TON, and Si, and fewer
607 sites at the upper end of the nutrient and EC gradients. Further refinement of the EC transfer functions
608 could be achieved with more evenly distributed sampling across the environmental gradient. The ML
609 model, with higher r_{boot}^2 , appears more capable of addressing these issues and maintains more
610 consistent predictive power across the EC range. This is likely due to its explicit curve-fitting approach.
611 By estimating individual species optima and tolerances, ML can better represent asymmetric or skewed
612 response curves (Birks, 2012). The ML transfer function is therefore considered the preferred model,
613 although both WA and ML are robust based on comparable RMSEP.

614 **4.5 Future applications for reconstructing past climate changes**

615 Incorporating diatom data with seasonal and multi-year hydrogeochemical data provides a unique
616 opportunity to comprehensively understand diatom-environment responses. By quantifying temporal
617 variability in hydrogeochemical processes, including the role of evaporation, this study strengthens
618 confidence that EC reflects SHW-driven sea-spray inputs rather than local lake hydrogeochemical
619 processes. This hydrological context is critical for interpreting diatom-environment relationships and
620 ensuring the reliability of EC as a proxy for past SHW behaviour, providing a strong foundation for future
621 palaeoclimate reconstructions. The resulting diatom-conductivity model provides a robust and
622 ecologically grounded framework for reconstructing long-term SHW variability on Macquarie Island and
623 establishes an important benchmark for sub-Antarctic palaeoclimate comparisons across the region.

624

625 By capturing ecological baseline and recovered conditions, the model developed in the present study
626 offers an improved foundation for assessing long-term wind-driven variability, as it reduces ecological



627 noise associated with past disturbance. When applied in parallel with other proxies, such as isotopic or
628 geochemical indicators (e.g. mercury and mercury isotopes Schneider et al., 2024), these
629 reconstructions will contribute to a more comprehensive understanding of past SHW dynamics and their
630 role in modulating Southern Hemisphere mid-high latitude climate, thereby providing context for
631 understanding future changes. Furthermore, a multiproxy approach will be valuable to independently
632 reconstruct other climatic factors such as precipitation which may also modify EC signals through dilution.

633 **5 Conclusion**

634 This study aimed to update and re-evaluate the reliability of diatom–conductivity models as a proxy for
635 reconstructing SHW variability on Macquarie Island by analysing diatom–environment relationships in
636 the context of seasonal and multi-year water chemistry and isotopic analysis. Our results demonstrate
637 that although lake hydrogeochemical processes vary locally, they remain stable seasonally and between
638 years. Lakes near the west coast and on the western edge consistently reflect strong SSA influence, and
639 while short-term evaporative enrichment occurs during summer, it does not obscure the dominant signal
640 of SHW-driven SSA inputs. Accordingly, EC reliably reflects SSA deposition rather than internal lake
641 hydrogeochemical processes, providing a firm mechanistic basis for the use of EC as an indicator of
642 SSA deposition in palaeoclimate studies on Macquarie Island.

643

644 Diatom–environment relationships were found to be strong and ecologically coherent, supporting the
645 development of a robust diatom–conductivity transfer function. Importantly, this study highlights the need
646 for careful site selection, with lakes that demonstrate stable hydrogeochemical behaviour, clear SSA
647 influence, and limited local disturbance providing the most reliable archives for reconstructing past SHW
648 variability. The resulting transfer function offers a reliable tool for reconstructing long-term SHW
649 dynamics, supported by well-characterised modern hydrological controls. Together, these findings
650 establish Macquarie Island as a well-constrained system for SHW reconstructions and provide a strong
651 foundation for future palaeoclimate work across the sub-Antarctic region.

652

653 **Supplementary material**

654 The Diatom Catalogue and Species List can be accessed from DOI [10.5281/zenodo.18041221](https://doi.org/10.5281/zenodo.18041221)

655



656 **Data availability**

657 The raw data supporting the conclusion on this work is available on request.

658

659 **Author contributions**

660 Caitlin Selfe: Conceptualization; Data curation; Formal analysis; Investigation; Methodology; Validation;
661 Visualization; Writing - original draft; Writing - review & editing.

662 Karina Meredith: Supervision; Research design; Resources; Writing - review & editing

663 Liza McDonough: Resources; Writing - review & editing

664 Justine Shaw: Supervision; Writing - review & editing

665 Steve Roberts: Supervision; Writing - review & editing

666 Krystyna Saunders: Conceptualisation; Supervision; Resources; Funding acquisition; Writing - review
667 & editing

668 Competing interests: The contact author has declared that none of the authors has any competing
669 interests.

670

671

672 **Acknowledgments**

673 This work was supported by ARC SRIEAS Grant SR200100005 Securing Antarctica's Environmental
674 Future. CS was supported by an AINSE Ltd. Residential Student Scholarship and acknowledges help
675 undertaking fieldwork from Maggie Smith, Sam Beale, Jez Bird, and Adam Darragh. We thank the
676 Tasmanian Parks and Wildlife Service and Australian Antarctic Division (AAS 4628) for field support
677 and access to Macquarie Island. We also thank ANSTO laboratories for sample analysis, particularly
678 Chris Vardanega and Henri Wong. This work contributes to delivering the Australian Antarctic Science
679 Decadal Strategy, in particular the Climate System and Change key priority.

680 **References**

681 Andersen, T., Carstensen, J., Hernandez-Garcia, E., & Duarte, C. M. (2009). Ecological thresholds and regime shifts:
682 approaches to identification. *Trends in Ecology & Evolution*, 24(1), 49-57.

683 Biester, H., Keppler, F., Putschew, A., Martinez-Cortizas, A., & Petri, M. (2004). Halogen retention, organohalogens, and the
684 role of organic matter decomposition on halogen enrichment in two Chilean peat bogs. *Environmental science &*
685 *technology*, 38(7), 1984-1991.

686 Birks, H. J. B. (2012). Overview of numerical methods in palaeolimnology. In *Tracking environmental change using Lake*
687 *sediments: Data handling and numerical techniques* (pp. 19-92). Springer.



688 BOM. (2025). *Australian Bureau of Meteorology, Climate statistics for Australian locations*. Australian Bureau of Meteorology.
689 https://www.bom.gov.au/climate/averages/tables/cw_30004.shtml

690 Buckney, R. T., & Tyler, P. A. (1974). Reconnaissance limnology of Sub-Antarctic islands. II. Additional features of the chemistry
691 of Macquarie Island lakes and tarns. *Marine and Freshwater Research*, 25(1), 89-95.

692 Chau, J. H., Born, C., McGeoch, M. A., Bergstrom, D., Shaw, J., Terauds, A., Mairal, M., Le Roux, J. J., & Jansen van Vuuren,
693 B. (2019). The influence of landscape, climate and history on spatial genetic patterns in keystone plants (Azorella) on
694 sub-Antarctic islands. *Molecular Ecology*, 28(14), 3291-3305. <https://doi.org/https://doi.org/10.1111/mec.15147>

695 Evans, A. J. (1970). Some aspects of the ecology of a calanoid copepod, *Psuedoboekela brevicaudata*. Brady, 1875, on a
696 subantarctic island. *ANARE Scientific Reports, series B*, 1, *Zoology*, 100.

697 Fletcher, M.-S., Pedro, J., Hall, T., Mariani, M., Alexander, J. A., Beck, K., Blaauw, M., Hodgson, D. A., Heijnis, H., & Gadd, P.
698 S. (2021). Northward shift of the southern westerlies during the Antarctic Cold Reversal. *Quaternary Science Reviews*,
699 271, 107189.

700 Fogt, R. L., & Marshall, G. J. (2020). The Southern Annular Mode: variability, trends, and climate impacts across the Southern
701 Hemisphere. *Wiley Interdisciplinary Reviews: Climate Change*, 11(4), e652.

702 Frölicher, T. L., Sarmiento, J. L., Paynter, D. J., Dunne, J. P., Krasting, J. P., & Winton, M. (2015). Dominance of the Southern
703 Ocean in anthropogenic carbon and heat uptake in CMIP5 models. *Journal of Climate*, 28(2), 862-886.

704 Gat, J. R. (1996). Oxygen and hydrogen isotopes in the hydrologic cycle. *Annual Review of Earth and Planetary Sciences*,
705 24(1), 225-262.

706 Gerritse, R. G., & George, R. J. (1988). The role of soil organic matter in the geochemical cycling of chloride and bromide.
707 *Journal of Hydrology*, 101(1-4), 83-95.

708 Gillett, N. P., Kell, T. D., & Jones, P. (2006). Regional climate impacts of the Southern Annular Mode. *Geophysical Research
709 Letters*, 33(23).

710 Goeyers, C., Vitt, D. H., & Van de Vijver, B. (2022). Taxonomic and biogeographical analysis of diatom assemblages from
711 historic bryophyte samples from Campbell Island (sub-Antarctic). *Plant Ecology and Evolution*, 155(1), 107-122.

712 Goldenberg Vilar, A., Donders, T., Cvetkoska, A., & Wagner-Cremer, F. (2018). Seasonality modulates the predictive skills of
713 diatom based salinity transfer functions. *PLoS One*, 13(11), e0199343. <https://doi.org/10.1371/journal.pone.0199343>

714 Gonfiantini, R., Wassenaar, L. I., & Araguas-Araguas, L. J. (2020). Stable isotope fractionations in the evaporation of water:
715 The wind effect. *Hydrological processes*, 34(16), 3596-3607.

716 Goyal, R., Sen Gupta, A., Jucker, M., & England, M. H. (2021). Historical and projected changes in the Southern Hemisphere
717 surface westerlies. *Geophysical Research Letters*, 48(4), e2020GL090849.

718 Gremmen, N. J., Van De Vijver, B., Frenot, Y., & Lebouvier, M. (2007). Distribution of moss-inhabiting diatoms along an
719 altitudinal gradient at sub-Antarctic îles Kerguelen. *Antarctic Science*, 19(1), 17-24.

720 Grose, M. R., Corney, S. P., Katzfey, J. J., Bennett, J. C., Holz, G. K., White, C. J., & Bindoff, N. L. (2013). A regional response
721 in mean westerly circulation and rainfall to projected climate warming over Tasmania, Australia. *Climate Dynamics*,
722 40(7), 2035-2048.

723 Guevara, S. R., Rizzo, A., Daga, R., Williams, N., & Villa, S. (2019). Bromine as indicator of source of lacustrine sedimentary
724 organic matter in paleolimnological studies. *Quaternary Research*, 92(1), 257-271.

725 IPCC. (2007). Climate change 2007: The physical science basis. *Agenda*, 6(07), 333.

726 IPCC. (2023). Summary for Policymakers. In C. Intergovernmental Panel on Climate (Ed.), *Climate Change 2021 – The Physical
727 Science Basis: Working Group I Contribution to the Sixth Assessment Report of the Intergovernmental Panel on
728 Climate Change* (pp. 3-32). Cambridge University Press. <https://doi.org/DOI: 10.1017/9781009157896.001>

729 Jones, J. M., Gille, S. T., Goosse, H., Abram, N. J., Canziani, P. O., Charman, D. J., Clem, K. R., Crosta, X., de Lavergne, C.,
730 Eisenman, I., England, M. H., Fogt, R. L., Frankcombe, L. M., Marshall, G. J., Masson-Delmotte, V., Morrison, A. K.,
731 Orsi, A. J., Raphaël, M. N., Renwick, J. A., . . . Vance, T. R. (2016). Assessing recent trends in high-latitude Southern
732 Hemisphere surface climate. *Nature Climate Change*, 6(10), 917-926. <https://doi.org/10.1038/nclimate3103>

733 Juggins, S. (2003). *C2 User Guide. Software for ecological and palaeoecological data analysis and visualisation*. In University
734 of Newcastle.

735 Juggins, S. (2013). Quantitative reconstructions in palaeolimnology: new paradigm or sick science? *Quaternary Science
736 Reviews*, 64, 20-32. <https://doi.org/https://doi.org/10.1016/j.quascirev.2012.12.014>

737 Keenan, H. M. (1995). Modern and fossil terrestrial and freshwater habitats on subantarctic Macquarie Island. *Macquarie
738 University, Thesis*. <https://doi.org/https://doi.org/10.25949/24796983.v1>

739 Kennedy, B., & Buckley, Y. M. (2021). Use of seasonal epilithic diatom assemblages to evaluate ecological status in Irish lakes.
740 *Ecological Indicators*, 129, 107853. <https://doi.org/https://doi.org/10.1016/j.ecolind.2021.107853>

741 Keppler, L., & Landschützer, P. (2019). Regional wind variability modulates the Southern Ocean carbon sink. *Scientific Reports*,
742 9(1), 7384.



743 Kilian, R., & Lamy, F. (2012). A review of Glacial and Holocene paleoclimate records from southernmost Patagonia (49–55°S).
744 *Quaternary Science Reviews*, 53, 1-23. <https://doi.org/https://doi.org/10.1016/j.quascirev.2012.07.017>

745 Kong, Z., Prata, A., May, P., Purich, A., Huang, Y., & Siems, S. (2025). Intensifying precipitation over the Southern Ocean
746 challenges reanalysis-based climate estimates—Insights from Macquarie Island's 45-year record. *EGUsphere*, 2025,
747 1-25.

748 Le Quéré, C., Raupach, M. R., Canadell, J. G., Marland, G., Bopp, L., Ciais, P., Conway, T. J., Doney, S. C., Feely, R. A.,
749 Foster, P., Friedlingstein, P., Gurney, K., Houghton, R. A., House, J. I., Huntingford, C., Levy, P. E., Lomas, M. R.,
750 Majkut, J., Metzl, N., . . . Woodward, F. I. (2009). Trends in the sources and sinks of carbon dioxide. *Nature Geoscience*,
751 2(12), 831-836. <https://doi.org/10.1038/ngeo689>

752 Le Quéré, C., Rödenbeck, C., Buitenhuis, E. T., Conway, T. J., Langenfelds, R., Gomez, A., Labuschagne, C., Ramonet, M.,
753 Nakazawa, T., Metzl, N., Gillett, N., & Heimann, M. (2007). Saturation of the Southern Ocean CO₂ Sink Due to Recent
754 Climate Change. *Science*, 316(5832), 1735-1738. <https://doi.org/doi:10.1126/science.1136188>

755 le Roux, P. C., & McGeoch, M. A. (2008). Rapid range expansion and community reorganization in response to warming. *Global
756 Change Biology*, 14(12), 2950-2962. <https://doi.org/https://doi.org/10.1111/j.1365-2486.2008.01687.x>

757 Lee, J. E., & Chown, S. L. (2016). Range expansion and increasing impact of the introduced wasp *Aphidius matricariae* Haliday
758 on sub-Antarctic Marion Island. *Biological Invasions*, 18(5), 1235-1246. <https://doi.org/10.1007/s10530-015-0967-3>

759 Löffler, E. (1984). Macquarie Island: A wind-molded natural landscape in the subantarctic. *Polar Geography*, 8(4), 267-286.

760 Marchant, R., Kefford, B., Wasley, J., King, C., Doube, J., & Nugegoda, D. (2011). Response of stream invertebrate communities
761 to vegetation damage from overgrazing by exotic rabbits on subantarctic Macquarie Island. *Marine and Freshwater
762 Research*, 62(4), 404-413.

763 Marshall, G. J. (2003). Trends in the Southern Annular Mode from observations and reanalyses. *Journal of Climate*, 16(24),
764 4134-4143.

765 McBride, T. (2009). Freshwater diatoms on sub-antarctic Macquarie Island: an ecological survey of 14 lakes.

766 McBride, T. P., & Selkirk, J. M. (1998). Palaeolake diatoms on sub-Antratic Macquarie Island: Possible markers of climate
767 change. *Data Symposium*

768 Menviel, L. C., Spence, P., Kiss, A. E., Chamberlain, M. A., Hayashida, H., England, M. H., & Waugh, D. (2023). Enhanced
769 Southern Ocean CO₂ outgassing as a result of stronger and poleward shifted southern hemispheric westerlies.
770 *Biogeosciences*, 20(21), 4413-4431.

771 Meredith, K., Hollins, S., Hughes, C., Cendón, D., Hankin, S., & Stone, D. (2009). Temporal variation in stable isotopes (18O
772 and 2H) and major ion concentrations within the Darling River between Bourke and Wilcannia due to variable flows,
773 saline groundwater influx and evaporation. *Journal of Hydrology*, 378(3-4), 313-324.

774 Meredith, K. T., Saunders, K. M., McDonough, L. K., & McGeoch, M. (2022). Hydrogeochemical and isotopic baselines for
775 understanding hydrological processes across Macquarie Island. *Scientific Reports*, 12(1), 21266.
776 <https://doi.org/10.1038/s41598-022-25115-3>

777 Minvielle, M., & Garreaud, R. D. (2011). Projecting rainfall changes over the South American Altiplano. *Journal of Climate*,
778 24(17), 4577-4583.

779 Molén, M. O. (2024). Geochemical proxies: Paleoclimate or paleoenvironment? *Geosystems and Geoenvironment*, 3(1),
780 100238.

781 Mongwe, P., Gregor, L., Tjiputra, J., Hauck, J., Ito, T., Danek, C., Vichi, M., Thomalla, S., & Monteiro, P. M. S. (2024). Projected
782 poleward migration of the Southern Ocean CO₂ sink region under high emissions. *Communications Earth &
783 Environment*, 5(1), 232. <https://doi.org/10.1038/s43247-024-01382-y>

784 Nel, W., Hedding, D. W., & Rudolph, E. M. (2023). The sub-Antarctic islands are increasingly warming in the 21st century.
785 *Antarctic Science*, 35(2), 124-126.

786 Nicholson, S.-A., Whitt, D. B., Fer, I., du Plessis, M. D., Lebéhot, A. D., Swart, S., Sutton, A. J., & Monteiro, P. M. S. (2022).
787 Storms drive outgassing of CO₂ in the subpolar Southern Ocean. *Nature Communications*, 13(1), 158.
788 <https://doi.org/10.1038/s41467-021-27780-w>

789 Oksanen, J., Blanchet, F. G., Kindt, R., Legendre, P., Minchin, P. R., O'Hara, R., Simpson, G. L., Solymos, P., Stevens, M. H.
790 H., & Wagner, H. (2013). Package 'vegan'. *Community ecology package*, version, 2(9), 1-295.

791 Olivier, L., & Haumann, F. A. (2025). Southern Ocean freshening stalls deep ocean CO₂ release in a changing climate. *Nature
792 Climate Change*, 15(11), 1219-1225. <https://doi.org/10.1038/s41558-025-02446-3>

793 Perren, B. B., Hodgson, D. A., Roberts, S. J., Sime, L., Van Nieuwenhuyze, W., Verleyen, E., & Vyverman, W. (2020). Southward
794 migration of the Southern Hemisphere westerly winds corresponds with warming climate over centennial timescales
795 [Article]. *Communications Earth and Environment*, 1(1), Article 58. <https://doi.org/10.1038/s43247-020-00059-6>

796 Recasens, C., Ariztegui, D., Maidana, N. I., Zolitschka, B., & Team, P. S. (2015). Diatoms as indicators of hydrological and
797 climatic changes in Laguna Potrok Aike (Patagonia) since the Late Pleistocene. *Palaeogeography, Palaeoclimatology,
798 Palaeoecology*, 417, 309-319.



799 Roberts, D., McMinn, A., & Zwart, D. (2000). An initial palaeosalinity history of Jaw Lake, Bunger Hills based on a diatom–
800 salinity transfer function applied to sediment cores. *Antarctic Science*, 12(2), 172–176.

801 Rouault, M., Pohl, B., & Penven, P. (2010). Coastal oceanic climate change and variability from 1982 to 2009 around South
802 Africa. *African Journal of Marine Science*, 32(2), 237–246.

803 Sabbe, K., Vyverman, W., Ector, L., Wetzel, C. E., John, J., Hodgson, D. A., Verleyen, E., & Van de Vijver, B. (2019). On the
804 identity of *Navicula gottlandica* (Bacillariophyta), with the description of two new species *Navicula eileencoxiana* and
805 *Navicula bergstromiana* from the Australo-Pacific region. *Plant Ecology and Evolution*, 152(2), 313–326.
806 <https://www.jstor.org/stable/26672975>

807 Salinger, M., & Mullan, A. (1999). New Zealand climate: temperature and precipitation variations and their links with atmospheric
808 circulation 1930–1994. *International Journal of Climatology: A Journal of the Royal Meteorological Society*, 19(10),
809 1049–1071.

810 Saunders, K. M., Harrison, J. J., Hodgson, D. A., de Jong, R., Mauchle, F., & McMinn, A. (2013). Ecosystem impacts of feral
811 rabbits on World Heritage sub-Antarctic Macquarie Island: A palaeoecological perspective. *Anthropocene*, 3, 1–8.
812 <https://doi.org/https://doi.org/10.1016/j.ancene.2014.01.001>

813 Saunders, K. M., Hodgson, D. A., & McMinn, A. (2009). Quantitative relationships between benthic diatom assemblages and
814 water chemistry in Macquarie Island lakes and their potential for reconstructing past environmental changes [Article].
815 *Antarctic Science*, 21(1), 35–49. <https://doi.org/10.1017/S0954102008001442>

816 Saunders, K. M., Hodgson, D. A., McMurtrie, S., & Grosjean, M. (2015). A diatom-conductivity transfer function for reconstructing
817 past changes in the Southern Hemisphere westerly winds over the Southern Ocean [Article]. *Journal of Quaternary
818 Science*, 30(5), 464–477. <https://doi.org/10.1002/jqs.2788>

819 Saunders, K. M., Roberts, S. J., Perren, B., Butz, C., Sime, L., Davies, S., Van Nieuwenhuyze, W., Grosjean, M., & Hodgson,
820 D. A. (2018). Holocene dynamics of the Southern Hemisphere westerly winds and possible links to CO₂ outgassing
821 [Article]. *Nature Geoscience*, 11(9), 650–655. <https://doi.org/10.1038/s41561-018-0186-5>

822 Schneider, M. A., Schneider, L., Cadd, H., Thomas, Z. A., Martinez-Cortizas, A., Connor, S. E., Stannard, G. L., & Haberle, S.
823 G. (2024). Long-term mercury accumulation and climate reconstruction of an Australian alpine lake during the late
824 Quaternary. *Global and Planetary Change*, 240, 104539.
825 <https://doi.org/https://doi.org/10.1016/j.gloplacha.2024.104539>

826 Selkirk-Bell, J., & Selkirk, P. (2013). Vegetation-banked terraces on Subantarctic Macquarie Island: a reappraisal. *Arctic,
827 antarctic, and alpine research*, 45(2), 261–274.

828 Selkirk, P., Seppelt, R., & Selkirk, D. (1990). *Subantarctic Macquarie Island: environment and biology*. Cambridge University
829 Press.

830 Shakun, J. D., Clark, P. U., He, F., Marcott, S. A., Mix, A. C., Liu, Z., Otto-Bliesner, B., Schmittner, A., & Bard, E. (2012). Global
831 warming preceded by increasing carbon dioxide concentrations during the last deglaciation. *Nature*, 484(7392), 49–54.

832 Shi, G., Cai, W., Cowan, T., Ribbe, J., Rotstyn, L., & Dix, M. (2008). Variability and trend of North West Australia rainfall:
833 observations and coupled climate modeling. *Journal of Climate*, 21(12), 2938–2959.

834 Sterken, M., Verleyen, E., Jones, V., Hodgson, D., Vyverman, W., Sabbe, K., & Van de Vijver, B. (2015). An illustrated and
835 annotated checklist of freshwater diatoms (Bacillariophyta) from Livingston, Signy and Beak Island (Maritime Antarctic
836 Region). *Plant Ecology and Evolution*, 148(3), 431–455.

837 Sterken, M., Verleyen, E., Sabbe, K., Terryn, G., Charlet, F., Bertrand, S., Boës, X., Fagel, N., De Batist, M., & Vyverman, W.
838 (2008). Late Quaternary climatic changes in southern Chile, as recorded in a diatom sequence of Lago Puyehue (40–
839 40° S). *Journal of Paleolimnology*, 39(2), 219–235.

840 ter Braak, C. J., & Juggins, S. (1993). Weighted averaging partial least squares regression (WA-PLS): an improved method for
841 reconstructing environmental variables from species assemblages. *Hydrobiologia*, 269(1), 485–502.

842 Ter Braak, C. J., & Prentice, I. C. (1988). A theory of gradient analysis. In *Advances in ecological research* (Vol. 18, pp. 271–
843 317). Elsevier.

844 Thomas, Z. A., Cadd, H., Turney, C., Becerra-Valdivia, L., Haines, H. A., Marjo, C., Fogwill, C., Carter, S., & Brickle, P. (2025).
845 Westerly wind shifts drove Southern Hemisphere mid-latitude peat growth since the last glacial. *Nature Geoscience*.
846 <https://doi.org/10.1038/s41561-025-01842-w>

847 Toggweiler, J. R., Russell, J. L., & Carson, S. R. (2006). Midlatitude westerlies, atmospheric CO₂, and climate change during
848 the ice ages. *Paleoceanography*, 21(2).

849 Torgersen, T. (1984). Wind effects on water and salt loss in playa lakes. *Journal of Hydrology*, 74(1–2), 137–149.

850 Ummenhofer, C. C., & England, M. H. (2007). Interannual extremes in New Zealand precipitation linked to modes of Southern
851 Hemisphere climate variability. *Journal of Climate*, 20(21), 5418–5440.

852 Van de Vijver, B., Freynot, Y., & Beyens, L. (2002). Freshwater diatoms from Ile de la Possession (Crozet archipelago,
853 Subantartica). *Bibliotheca Diatomologica*, 46, 1–412.



854 Van de Vijver, B. (2012). *Aulacoseira principissa* sp. nov., a new 'centric' diatom species from the sub-Antarctic region.
855 *Phytotaxa*, 52, 33–42-33–42.

856 Van de Vijver, B. (2019). Revision of the *Psammothidium manguinii* complex (Bacillariophyta) in the sub-Antarctic Region with
857 the description of four new taxa. *Fottea*, 19(1), 90-106. <https://doi.org/10.5507/fot.2019.001>

858 Van Nieuwenhuyze, W. (2020). *Diatom species and limnological data from 64 lakes on subantarctic Marion Island (2011) [Data
859 set]* Version (Version 1.0)). <https://doi.org/https://doi.org/10.5285/1fa89ba7-a904-43a8-a98d-ff887584221a>

860 Verleyen, E., Hodgson, D. A., Vyverman, W., Roberts, D., McMinn, A., Vanhoutte, K., & Sabbe, K. (2003). Modelling diatom
861 responses to climate induced fluctuations in the moisture balance in continental Antarctic lakes. *Journal of
862 Paleolimnology*, 30, 195-215.

863